Miner Deposita (2008) 43:129–159
DOI 10.1007/s00126-006-0121-3

ARTICLE

Spatial and temporal zoning of hydrothermal alteration and mineralization in the Sossego iron oxide–copper–gold deposit, Carajás Mineral Province, Brazil: paragenesis and stable isotope constraints

Lena V. S. Monteiro · Roberto P. Xavier · Emerson R. de Carvalho · Murray W. Hitzman · Craig A. Johnson · Carlos Roberto de Souza Filho · Ignácio Torresi

Received: 10 January 2006 / Accepted: 10 December 2006 / Published online: 23 January 2007
© Springer-Verlag 2007

Abstract The Sossego iron oxide–copper–gold deposit (245 Mt @ 1.1% Cu, 0.28 g/t Au) in the Carajás Mineral Province of Brazil consists of two major groups of orebodies (Pista–Sequeirinho–Baiano and Sossego–Curral) with distinct alteration assemblages that are separated from each other by a major high angle fault. The deposit is located along a regional WNW–ESE-striking shear zone that defines the contact between metavolcano–sedimentary units of the ~2.76 Ga Itacaiúnas Supergroup and tonalitic to trondhjemitic gneisses and migmatites of the ~2.8 Ga Xingu Complex. The deposit is hosted by granite, granophyric granite, gabbro, and felsic metavolcanic rocks. The Pista–Sequeirinho–Baiano orebodies have undergone regional sodic (albite–hematite) alteration and later sodic–calcic (actinolite-rich) alteration associated with the formation of massive magnetite–(apatite) bodies. Both these alteration assemblages display ductile to ductile–brittle fabrics. They are cut by spatially restricted zones of potassic (biotite and potassium feldspar) alteration that grades outward to chlorite-rich assemblages. The Sossego–Curral orebodies contain weakly developed early albitic alteration and very poorly developed subsequent calcic–sodic alteration. These orebodies contain well-developed potassic alteration assemblages that were formed during brittle deformation that resulted in the formation of breccia bodies. Breccia matrix commonly displays coarse mineral infill suggestive of growth into open space. Sulfides in both groups of deposits were precipitated first with potassic alteration and more importantly with a later assemblage of calcite–quartz–epidote–chlorite. In the Sequeirinho orebodies, sulfides range from undeformed to deformed; sulfides in the Sossego–Curral orebodies are undeformed. Very late, weakly mineralized hydrolytic alteration is present in the Sossego/Currral orebodies. The sulfide assemblage is dominated by chalcopyrite with subsidiary siegenite, and millerite. Pyrrhotite and pyrite are minor constituents of ore in the Sequerinho orebodies while pyrite is relatively abundant in the Sossego–Curral bodies. Oxygen isotope partitioning between mineral pairs constrains temperatures in the deposit spatially and through time. In the Sequeirinho orebody, the early sodic–calcic alteration stage was characterized by temperatures exceeding 500°C and $\delta^{18}O_{H_2O}$ values for the alteration fluid of 6.9±0.9‰. Temperature declines outward and upward from the zone of most intense alteration. Paragenetically later copper–gold mineralization displays markedly lower tem-

Editorial handling: S. Hagemann

L. V. S. Monteiro (✉) · R. P. Xavier · E. R. de Carvalho · C. R. de Souza Filho · I. Torresi
Instituto de Geociências, Universidade Estadual de Campinas,
R. João Pandiá Calógeras, 51,
CEP 13083–970 Campinas, Sao Paulo, Brazil
e-mail: lena@ige.unicamp.br

M. W. Hitzman
Department of Geology and Geological Engineering,
Colorado School of Mines,
Golden, CO 80401, USA

C. A. Johnson
U.S. Geological Survey,
Box 25046, MS 963,
Denver, CO 80225, USA

peratures (<300°C) and was characterized by the introduction of ^{18}O-depleted hydrothermal fluids −1.8±3.4‰. The calculated δD_{H2O} and $\delta^{18}O_{H_2O}$ values suggest that the fluids that formed the early calcic–sodic alteration assemblage were of formational/metamorphic or magmatic origin. The decrease of $\delta^{18}O_{H_2O}$ values through time may reflect influx of surficially derived waters during later alteration and mineralization events. Influx of such fluids could be related to episodic fluid overpressure, resulting in dilution and cooling of the metalliferous fluid, causing deposition of metals transported as metal chloride complexes.

Keywords Sossego · Iron oxide–Cu–Au deposits · Alteration zoning · Stable isotopes · Carajás Mineral Province · Brazil

Introduction

The Sossego iron oxide–copper–gold (IOCG) mine, operated by the Companhia Vale do Rio Doce (CVRD) in the Carajás Mineral Province (CMP), Pará state, Brazil, was placed into production in 2004. The deposit has ore reserves of 245 Mt averaging 1.1% Cu and 0.28 g/t Au (Lancaster-Oliveira et al. 2000), which are contained primarily within two orebodies: Sequeirinho and Sossego.

Recent studies (Lancaster-Oliveira et al. 2000; Carvalho et al. 2004, 2005; Monteiro et al. 2004a,b; Villas et al. 2004, 2005; Souza et al. 2004) indicate that Sossego shares many attributes with other deposits from the CMP. This province contains the world's largest known concentration of large-tonnage IOCG deposits, such as Salobo (789 Mt @ 0.96% Cu, 0.52 g/t Au, 55 g/t Ag; Souza and Vieira 2000), Cristalino (500 Mt @ 1.0% Cu; 0.3 g/t Au; Huhn et al. 1999), Igarapé Bahia/Alemão (219 Mt @ 1.4% Cu, 0.86 g/t Au; Tallarico et al. 2005), Gameleira (100 Mt @ 0.7% Cu; Rigon 2000), and Alvo 118 (70 Mt @ 1.0% Cu, 0.3 g/t Au; Rigon 2000).

Despite the importance of the Carajás IOCG deposits, geological information about them is relatively scarce. This detailed study of the Sossego deposit will allow comparison to other IOCG deposits.

Detailed petrographic studies permitted to outline a consistent paragenetic sequence and the spatial and temporal zoning of alteration and mineralization. This paper also presents the results of a stable isotopic study of alteration minerals and sulfides at Sossego. The data indicate that the alteration minerals within the deposit preserve a record of decreasing temperature through time. The results also suggest the involvement of both deep-seated, formational/metamorphic fluids possibly with magmatic contribution, and meteoric-hydrothermal fluids in the formation of the Sossego deposit.

Geological setting of the Carajás Mineral Province

The Carajás Mineral Province (CMP) is located in the southern part of the Amazon Craton, which is one of the largest cratonic areas in the world. This province is divided into two tectonic blocks, the southern Rio Maria greenstone terrain (Huhn et al. 1988), and the northern Itacaúnas Shear Belt (Araújo et al. 1988). The oldest units in the province occur in the southern block and encompass the 2.98–2.90 Ga Andorinha Supergroup greenstone belt sequences (Docegeo 1988; Huhn et al. 1988; Araújo et al. 1988; Faraco et al. 1996) and the Arco Verde Tonalite (2.97–2.90 Ga; Pimentel and Machado 1994). These sequences were intruded by 2.96 Ga trondjemites, 2.87 Ga late-tectonic I-type calc–alkaline Rio Maria-type granodiorite (Dardenne and Schobbenhaus 2001), 2.81 Ga granites, and 2.54–2.52 Ga leucogranites (Macambira and Lafon 1995).

Within the northern block of the CMP (Fig. 1), the Archean basement comprises granulites of the Pium Complex (~3.0 Ga; Rodrigues et al. 1992) and tonalitic to trondhjemitic gneiss and migmatites of the Xingu Complex (~2.8 Ga; Machado et al. 1991). The basement rocks are overlain by metavolcanic–sedimentary units of the Rio Novo Group (Hirata et al. 1982) and the 2.76 Ga Itacaiúnas Supergroup (Igarapé Salobo, Igarapé Pojuca, Grão Pará, and Igarapé Bahia Groups: Wirth et al. 1986; Docegeo 1988; Machado et al. 1991), which form the Archean Carajás Basin. The Igarapé Salobo Group consists of paragneiss, amphibolite, quartzite, meta-arkose, and iron formation, whereas the Igarapé Pojuca Group contains basic metavolcanic rocks, pelitic schists, amphibolites, and iron formations metamorphosed to greenschist to amphibolite facies. The Grão Pará Group comprises lower greenschist facies metamorphic units including metabasalts, felsic metavolcanic rocks, and iron formations. Greenschist facies metavolcanic, metapyroclastic, and metasedimentary rocks, including iron formations, define the Igarapé Bahia Group.

The Itacaiúnas Supergroup hosts all the Carajás IOCG deposits and is thought to have been deposited in a marine rift environment (Wirth et al. 1986; Docegeo 1988; Lindenmayer 1990; Dardenne and Schobbenhaus 2001). The metamorphism and deformation of this supergroup has been attributed to the development of the 2.7 Ga Itacaiúnas sinistral strike-slip ductile shear zone (Holdsworth and Pinheiro 2000) and to the Cinzento and Carajás sinistral ductile–brittle to brittle transcurrent fault systems (2,581–2,519 Ma; Machado et al. 1991). The Itacaiúnas Supergroup is overlain by an extensive succession of Archean (2,681±5 Ma; Trendall et al. 1998) marine to fluvial sandstones and siltstones, known as the Rio Fresco Group (Docegeo 1988) or the Águas Claras Formation (Nogueira 1985; Araújo et al. 1988).

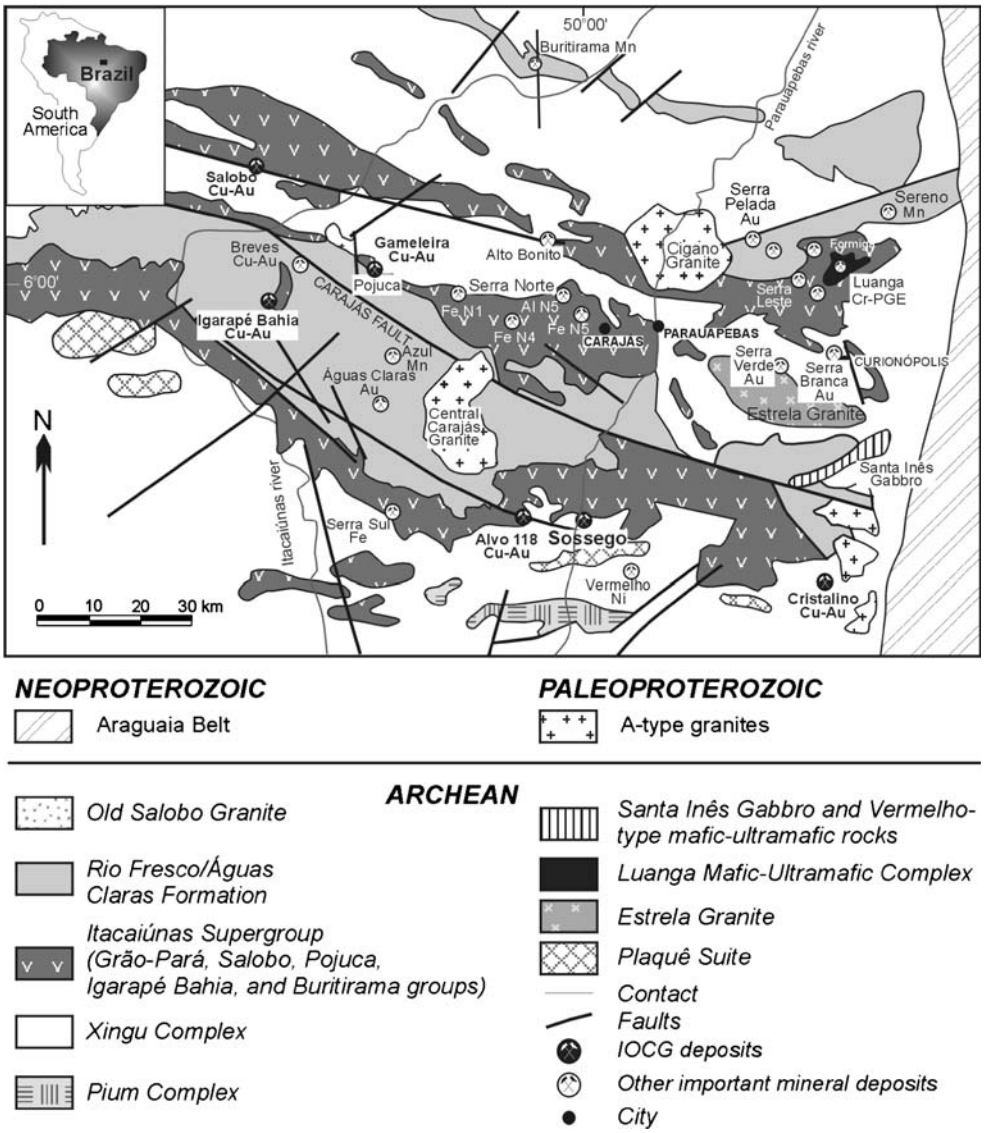

Fig. 1 Geological map of the Carajás Mineral Province (Docegeo 1988; Dardenne and Schobbenhaus 2001)

Syntectonic alkaline granites (2.76–2.74 Ga Estrela Granite Complex, Plaquê Suite, Planalto and Serra do Rabo; Dall'Ágnol et al. 1997; Barros et al. 2001) intrude the Itacaiúnas metavolcano–sedimentary sequence. Other Archean intrusions include the Luanga (2,763±6 Ma, Machado et al. 1991), Vermelho, Onça, and Jacaré–Jacarezinho mafic–ultramafic layered complexes, as well as 2.76–2.65 Ga gabbro dikes and sills (Galarza et al. 2003; Pimentel et al. 2003). Geochronological and geochemical constraints, including Nd isotope geochemistry, suggest that the ~2.76 Ga gabbros and the Itacaiúnas Supergroup mafic metavolcanic units are roughly coeval and cogenetic (Galarza et al. 2003; Pimentel et al. 2003). Late Archean alkaline, metaluminous granite (e.g., Old Salobo, 2,573± 2 Ma; Machado et al. 1991; Itacaiúnas, 2,560±37 Ma; Souza et al. 1996) also occur in the province. Paleoproterozoic magmatism is widespread throughout the CMP and is represented by within-plate A-type, alkaline to subalkaline granites (~1.88 Ga Serra dos Carajás, Cigano, Cigano, Pojuca, Young Salobo, Musa, Jamon, Seringa, Velho Guilherme, and Breves granites; Dall'Agnoll et al. 1994; Tallarico et al. 2004).

Ore deposits of the Carajás Mineral Province

The CMP contains a number of different ore deposit types and represents one of the best-endowed mineral districts in the world (Villas and Santos 2001; Fig. 1). Small, shear-zone-related, lode-type gold and Au–Cu–Bi–Mo deposits (Oliveira and Leonardos 1990; Leonardos et al. 1991; Silva and Cordeiro 1998) occur in the southern portion of the CMP. The northern portion of the CMP contains the world-class Carajás iron deposits (e.g., Serra Norte, Serra Sul; Beisiegel et al. 1973; Dalstra and Guedes 2004) in rocks of the 2.76 Ga Itacaiúnas Supergroup, which have estimated

reserves of 18 billion tonnes @ 63% Fe, as well as iron oxide-poor Cu–Mo–Au deposits (e.g., Serra Verde; Villas and Santos 2001) in metavolcanic rocks of the Rio Novo Group close to the contact with the 2.76 Ga Estrela Granite (Marschik et al. 2002). The CMP also has chrome–PGE deposits (e.g., Luanga) and lateritic nickel deposits (e.g., Vermelho, Puma–Onça) associated with mafic–ultramafic complexes (Bernadelli et al. 1983; Suita 1988; Costa 1997).

The ~2.68 Ga Águas Claras Formation in the central and northern CMP contains the Azul and Sereno manganese deposits (Coelho and Rodrigues 1986) and intrusion-related Cu–Au–(Mo–W–Bi–Sn) and W deposits associated with the 1.88 Ga anorogenic granite intrusions (Cordeiro and Silva 1986; Tallarico et al. 2004; Xavier et al. 2005). The Águas Claras Formation also hosts the Serra Pelada/Serra Leste Au–Pd–Pt deposit (Meireles and Silva 1988; Tallarico et al. 2000; Moroni et al. 2001; Cabral et al. 2002), which became famous due to a spectacular gold rush in the early 1980s.

The CMP also contains the world's largest known concentration of large-tonnage IOCG deposits (e.g., Sossego, Salobo, Igarapé Bahia, Alemão, Cristalino, Gameleira, and Alvo 118; Table 1). While geological information about some of these deposits is still preliminary (e.g., Cristalino and Alvo 118), a large database exists for the Igarapé Bahia and Salobo deposits. However, descriptions are ambiguous and interpretations are controversial (Villas and Santos 2001). The Carajás IOCG deposits display a number of similarities including: (1) variable host rock lithologies, in all cases including metavolcano–sedimentary units of the ~2.76 Ga Itacaiúnas Supergroup; (2) association with shear zones; (3) proximity to intrusions of different compositions (granite, diorite, gabbro, rhyolitic, or dacitic porphyry dikes); (4) intense hydrothermal alteration including sodic, sodic–calcic or potassic assemblages, together with chloritization, tourmalinization, and silicification; (5) magnetite formation followed by sulfide precipitation; and (6) a wide range of fluid inclusion homogenization temperatures (100–570°C) and salinities (0 to 69 wt% NaCl eq.) in ore-related minerals (Table 1).

Major differences among Carajás IOCG deposits include distinct hydrothermal alteration assemblages (e.g., high temperature silicates, such as fayalite and almandine, present only at Salobo) and ore minerals (e.g., chalcopyrite–chalcocite–bornite at Salobo; chalcopyrite ± chalcocite–digenite–covellite at Igarapé Bahia; and chalcopyrite–pyrite in the Sossego, Cristalino, and Alvo 118 deposits).

Geochronological data from the Carajás IOCG deposits point to at least three possible Archean and Paleoproterozoic metallogenetic events: (1) ~2.76 Ga (Galarza 2003); (2) ~2.57 Ga (Réquia et al. 2003; Tallarico et al. 2005; and (3) ~1.88 Ga (Pimentel et al. 2003). Most genetic models for the IOCG deposits emphasize the importance of Late Archean (~2.57 Ga) and/or Paleoproterozoic (~1.88 Ga) granitic intrusive activity for the establishment of extensive magmatic-hydrothermal systems (e.g., Tallarico et al. 2005; Tavaza and Oliveira 2000; Réquia et al. 2003; Pimentel et al. 2003; Lindenmayer 2003). However, syngenetic volcanogenic models (Lindenmayer 1990; Villas and Santos 2001; Dreher 2004; Dreher and Xavier 2005) have also been proposed for the genesis of the Salobo and Igarapé Bahia deposits.

Materials and methods

Documentation of the paragenetic sequence of hydrothermal alteration and mineralization in the Sossego deposit was carried out using mapping at the mine site and the surrounding areas, detailed drill core descriptions of 16 holes, petrographic studies under transmitted and reflected light, cathodoluminescence, and scanning electronic microscopy, and electron microprobe analysis. Stable isotope compositions were determined on 127 mineral separates, which were obtained by using a dental drill under a binocular microscope and by handpicking.

Stable isotope analyses of calcite, sulfides, and apatite samples were conducted at the Colorado School of Mines, USA, under the supervision of Dr. John Humphrey. Carbonate analyses were obtained using a MultPrep autosampler, which provides high-precision dual-inlet analysis of carbon and oxygen isotopes in carbonate samples (10 to 100 μg) through acid digestion. Sulfur isotopic analyses of sulfide samples (10 to 100 μg) were carried out using an Eurovector elemental analyzer, which generates SO_2 gas by combustion, purifies the gas by passing it through a chromatographic column, and then delivers it to the mass spectrometer. Oxygen isotope analyses of apatite were made using a Hekatech pyrolysis device.

Mass spectrometric measurements were made using a GV IsoPrime mass spectrometer. Oxygen and carbon isotope results are expressed in conventional delta (δ) notation, as per mil (‰), and are reported relative to the Vienna Standard Mean Ocean Water (VSMOW) and Pee Dee Belemnite (PDB) standards, respectively. Sulfur isotopic compositions are reported relative to the Cañon Diablo Troilite (CDT) standard.

Oxygen and hydrogen isotope analyses of oxides and silicates were carried out at the U.S. Geological Survey, Denver, USA. Oxygen isotope analyses were obtained using the method of Clayton and Mayeda (1963). Silicates, except epidote, were reacted overnight with BrF_5 at 580°C. Magnetite and epidote were reacted with BrF_5 for 2 days at 620°C. Hydrogen isotope analyses were conducted by heating samples under vacuum, passing the evolved gases over hot cupric oxide, and then converting the resulting

Table 1 Main characteristics of the IOCG deposits of the Carajás Mineral Province

Deposit	Reserve	Host rocks	Intrusive rocks	Hydrothermal alteration	Ore morphology	Ore mineralogy	Fluid inclusion (T=°C; salinity =wt% eq. NaCl)	Stable Isotopes (‰)	Mineralization age (Ma)
Sossego	245 Mt @ 1.1% Cu, 0.28 g/t Au (1)	Granite, felsic metavolcanic rocks, granophyric granite, gabbro (2)	Gabbro; acid intrusive rocks, diabase dikes (2, 3)	Na, Na–Ca, K alterations, chloritization, carbonatization (2, 3)	Crackle breccias, veins infilling (2, 3)	Ccp, Mag, Py, Sig; Mil; Hes; Hem; Sp (2, 3)	1. Th=102–312; salinity=0–23 Th= 200–570; salinity=32–69 (2)	$\delta^{34}S_{sulfides}$=2.2 to 7.6; $\delta^{18}O_{fluid}$=15.4 to −5.0 (3)	2.2–2.3 Ga Ar–Ar Act (4)
Salobo	789 Mt @ 0.96% Cu, 0.52 g/t Au (10)	Metadacite, amphibolites, metagraywackes iron formation (5, 6)	2.57 Ga and 1.88 Ga granites (6)	Na–, K– and Fe–K alterations (Kfs; Bt; Gr; Fa; Alm; All; Mag; Hast; Tur; Zr); Propylitic (6)	Pod or lens like bodies controlled by shear zone (6)	Mag, Bn; Ccp; Cc; Mo; Co-pen; Ilm; Cov; Dig; Hem; Cu (5, 6)	1. CH_4<10 mol%); 2. Th=360; Salinity= 35–58 3. Th=133–270; salinity: 1–29 (5)	$\delta^{34}S_{sulfides}$=0.2 to 1.6; $\delta^{18}O_{fluid}$=6.6 to12.1 (5)	2,579±71 Pb–Pb sulfides 2,576± 8 Re–Os Mo (5)
Igarapé Bahia/ Alemão	Alemão: 170 Mt @ 1.5% Cu; 0.8 g/t Au (7)	Metavolcanic, metavolcaniclastic metasedimentary rocks, BIF (7, 8)	2.76 Ga quartz diorite (8)	Chloritization; Tourmalinization; (Fe)–K alteration; Carbonatization; Na-Ca alteration (8, 9)	Breccia zones, dissemination veins (8, 9)	Ccp; Cc; Dig; Cov; Bn; Py, Mo; Cob; Hes (8, 9)	Main mineralization: Th=160 to 330; salinity: 5–45; late veins: Th=120 to 500; salinity: 2–60 (11, 12)	$\delta^{13}C$ carb=−6 to −15; $\delta^{18}O$ carb=2 to 20; $\delta^{34}S_{sulfides}$=−2.1 to 5.6 (12, 9)	2,772±46 Pb–Pb Ccp (10) 2,575±12 SHRIMP U–Pb Monazite (8)
Gameleira	100 Mt @ 0.7 % Cu (17)	Mafic to intermediate metavolcanic rocks, biotite schists, BIF (7)	2.70 Ga gabbro; 1.87 Ga and 1.58 Ga Gameleira granites (7)	K-alteration (Bt; Alm; Qtz; Ab; Tur; Ti; Ilm; Mag; Scp; Ap; Uran) (14, 15)	Stratabound, disseminated veins in shear zone (14)	Ccp; Py, Mo; Co-pen; Cob; Bn; Po; Au; Cub; Mag, Hem (14, 15)	1. Th=80–160; salinity: 8–21 2. Satured inclusions: Th=200–400 (14)	$\delta^{34}S_{sulfides}$=3.1 to 4.8; $\delta^{18}O_{carb}$=8.9 to 10; $\delta^{13}C_{carb}$=−8.4 to −9.5 (15)	1,734±8 Ar–Ar (K alteration) 1,700± 31 Sm–Nd ore (16)
Alvo 118	70 Mt @ 1.0% Cu; 0.3 g/t Au (13)	Mafic metavolcanic and metapyroclastic rocks, BIF	2.74 Ga tonalite; 2.65 Ga rhyolite; 2.64 dacite(11)	K-alteration, chloritization, silicification, carbonatization (17)	Hydraulic breccias, vein and fracture infilling (17)	Mag; Ccp, Py, Bn (17)			1,869±7; 1,869±7 (SHRIMP Pb–Pb Xe) (8)
Cristalino	500 Mt @ 1.0% Cu; 0.3 g/t Au (18)	Intermediate to felsic metavolcanic rocks, iron formations (18)	2.74 Ga diorite/ quartz diorite (18)	K–, Na– and Fe-alteration, chloritization, carbonatization (18)	Stockwork , fracture filling breccia (18)	Ccp; Py; Au; Bra; Cob; Mil; Va (18, 19)			2,719±36 Pb–Pb Ccp and Py (19)

Ab albite, *Act* actinolite, *All* allanite, *Alm* almandine, *Ap* apatite, *Bt* biotite, *Bn* bornite, *Bra* bravoite, *Cal* calcite, *Cc* chalcocite, *Ccp* chalcopyrite, *Chl* chlorite, *Co-pen* Co-pentlandite, *Cob* cobaltite, *Cov* covellite, *Cu* native copper, *Cub* cubanite, *Dig* digenite, *Ep* epidote, *Fa* Fayalite, *Fl* fluorite, *Gr* grunerite, *Has* hastingsita, *Hem* hematite, *Hes* hessite, *Ilm* ilmenite, *Kfs* K feldspar, *Mag* magnetite, *Mil* millerite, *Mo* molibdenite, *Ms* muscovite, *Py* pyrite, *Po* pyrrhotite, *Qtz* quartz, *Sig* siegenite, *Scp* scapolite, *Ser* sericite, *Sp* sphalerite, *St* stilpnomelane, *Ti* titanite, *Tur* tourmaline, *Uran* uraninite, *Va* vaesite, *Xe* xenotime, *Zr* zircon, *(1)* (http://www.vale.com.br/Julho/2004); Lancaster-Oliveira et al. (2000), *(2)* Carvalho et al. (2004, 2005), *(3)* Monteiro et al. (2004a,b), Monteiro et al. (submitted); this work, *(4)* Marschik and Leveille (2001), *(5)* Réquia and Xavier (1995); Réquia and Fontboté (2001); Réquia et al. (2003), *(6)* Lindenmayer (1990), *(7)* Galarza (2003), *(8)* Tallarico et al. (2005), *(9)* Tavaza and Oliveira (2000), *(10)* Dardenne and Schobbenhus (2001), *(11)* Almada (1998), *(12)* Dreher (2004), *(13)* Rigon et al. (2000), *(14)* Ronchi et al. (2000), *(15)* Lindenmayer et al. (2002), *(16)* Pimentel et al. (2003), *(17)* Albuquerque et al. (2001), *(18)* Huhn et al. (1999, 2000), *(19)* Soares et al. (2001)

H_2O to H_2 for mass spectrometry using zinc. Mass spectrometric measurements were made using a Finnigan MAT 252. Results are expressed in delta (δ) notation, as per mil (‰), relative to Vienna Standard Mean Ocean Water (VSMOW). Reproducibility was±0.2‰ for $\delta^{18}O$ and±5‰ for δD.

The Sossego iron oxide–copper–gold deposit

Geologic setting

The Sossego deposit occurs along a WNW–ESE-striking, 60 km-long belt of regional shearing that defines the southern contact between the 2.76 Ga Itacaiúnas Supergroup (Machado et al. 1991; Wirth et al. 1986) and the basement, represented by tonalitic to trondhjemitic gneisses and migmatites of the ~2.8 Ga Xingu Complex (Machado et al. 1991) (Fig. 1). In the Sossego deposit area, this shearing is represented by meter- to centimeter-wide mylonitic zones marked by intense silicification. This shear zone is regionally crosscut by N- and NW-striking faults. In the Sossego deposit area, the shear zone is also cut by a dextral system of transcurrent brittle–ductile E–W to NE–SW-striking subvertical dipping faults (Fig. 2a), which appear to delineate mineralized zones (Morais and Alkmim 2005).

In the Sossego area, granite, granophyric granite, gabbro intrusions, and late dacite porphyry dikes cut Xingu Complex basement and Itacaiúnas metavolcanic rocks. Their exact age of emplacement has not been determined. However, the granite, granophyric granite and gabbro have been altered by the Sossego hydrothermal system, indicating emplacement before 2.2 Ga (Marschik and Leveille 2001; Table 1). These

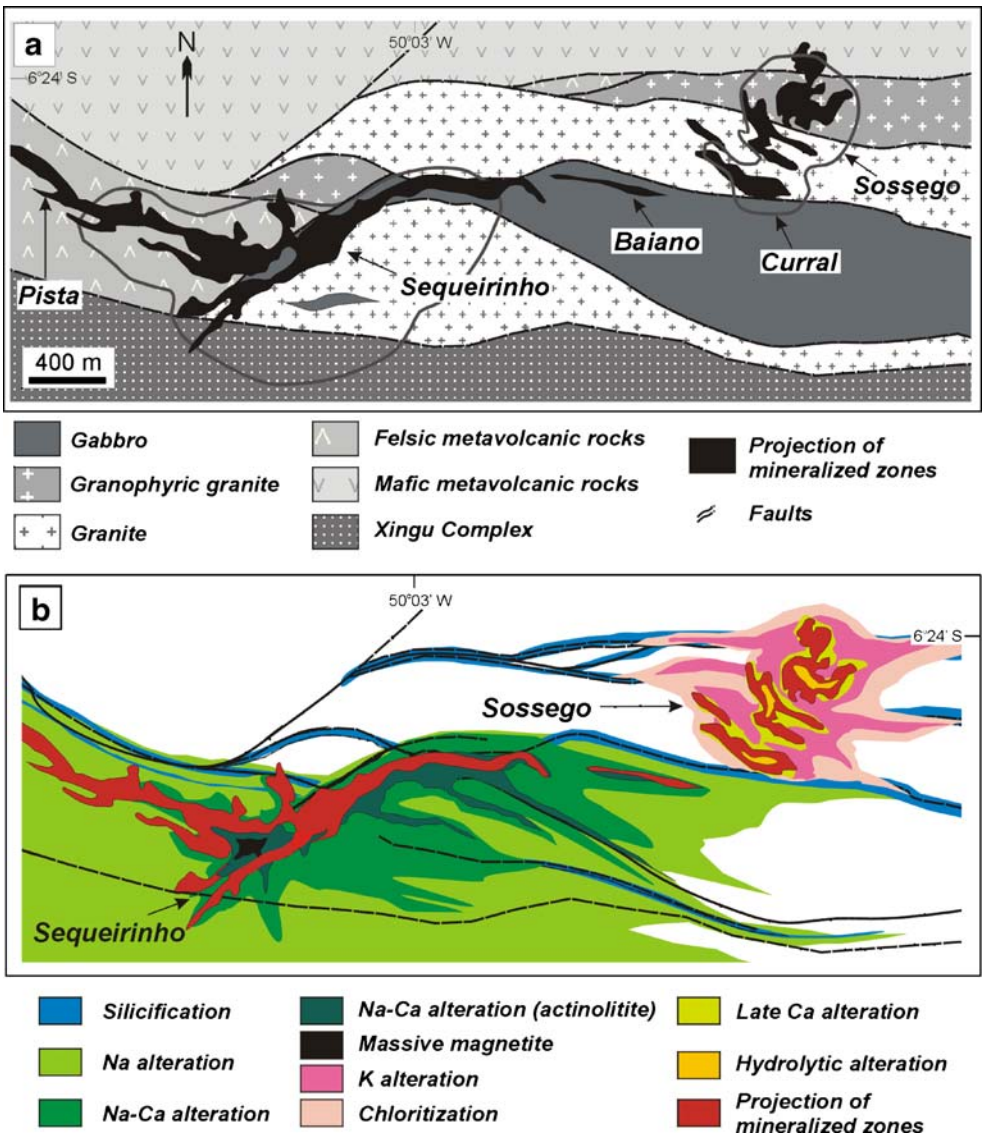

Fig. 2 **a** Simplified geologic map of the Sossego area and location of the Sequeirinho, Pista, Curral, Baiano, and Sossego orebodies (modified from Companhia Vale do Rio Doce); **b** schematic distribution of the hydrothermal alteration zones in the Sossego deposit

intrusive rocks are elongated in a WNW–ESE direction (Fig. 2a) concordant with the regional structures (Fig. 1). Late NW-oriented, unaltered diabase dikes crosscut shear zones, faults, and all other intrusive units.

The Sossego deposit comprises, from west to east, the Pista, Sequeirinho, Baiano, Curral, and Sossego orebodies (Fig. 2). The Sequeirinho and Sossego orebodies represent the bulk of resources, with 85 and 15% of the ore reserves, respectively. All of the orebodies occur in the hanging wall of major E–W to NE–SW-trending, high angle faults (Fig. 3). Intense hydrothermal alteration and mineralization is generally restricted to within several hundred meters of these faults. Rocks in the immediate footwalls of the faults are intensely mylonitized and display biotite–tourmaline–scapolite alteration and silicification near the fault contacts. Individual orebodies at Sossego display different styles and intensities of hydrothermal alteration.

Weakly altered felsic metavolcanic rocks in the Sossego deposit area are dacitic in composition. They are dark gray in color, fine-grained, and contain feldspar phenocrysts in a fine-grained matrix of microcrystalline quartz and albite. The felsic metavolcanic sequence contains lenses of metamorphosed ultramafic rocks. These fine-grained rocks are green in color and are composed of serpentine with remnants of olivine and minor disseminated chromite partially rimmed and replaced by magnetite. Where mylonitized, the ultramafic rocks have been converted to talc.

Weakly altered granite in the Sossego area is gray and medium-grained. The rock contains quartz, potassium feldspar, plagioclase, and minor biotite. Weakly altered granophyric granite is dark gray and contains blue quartz crystals up to 0.5 mm in diameter, as well as microcline and plagioclase phenocrysts in a fine-grained quartz-feldspar groundmass. Micrographic intergrowths of albitized K-feldspar, quartz, and spherulitic structures (represented by radial aggregates of quartz and feldspar) are typical of this rock.

Gabbro intrudes both granite and granophyric granite. The gabbro is green and medium- to coarse-grained. These intrusive rocks are equigranular, display subophitic texture, and are composed of intensely saussuritized plagioclase together with remnants of pyroxene and hornblende. The gabbro is commonly intensely altered to coarse-grained hydrothermal hastingsite and actinolite.

The gabbros are cut by brownish-colored dacitic and rhyolitic porphyry dikes composed of millimeter-size phenocrysts of K-feldspar, plagioclase, quartz, and oriented

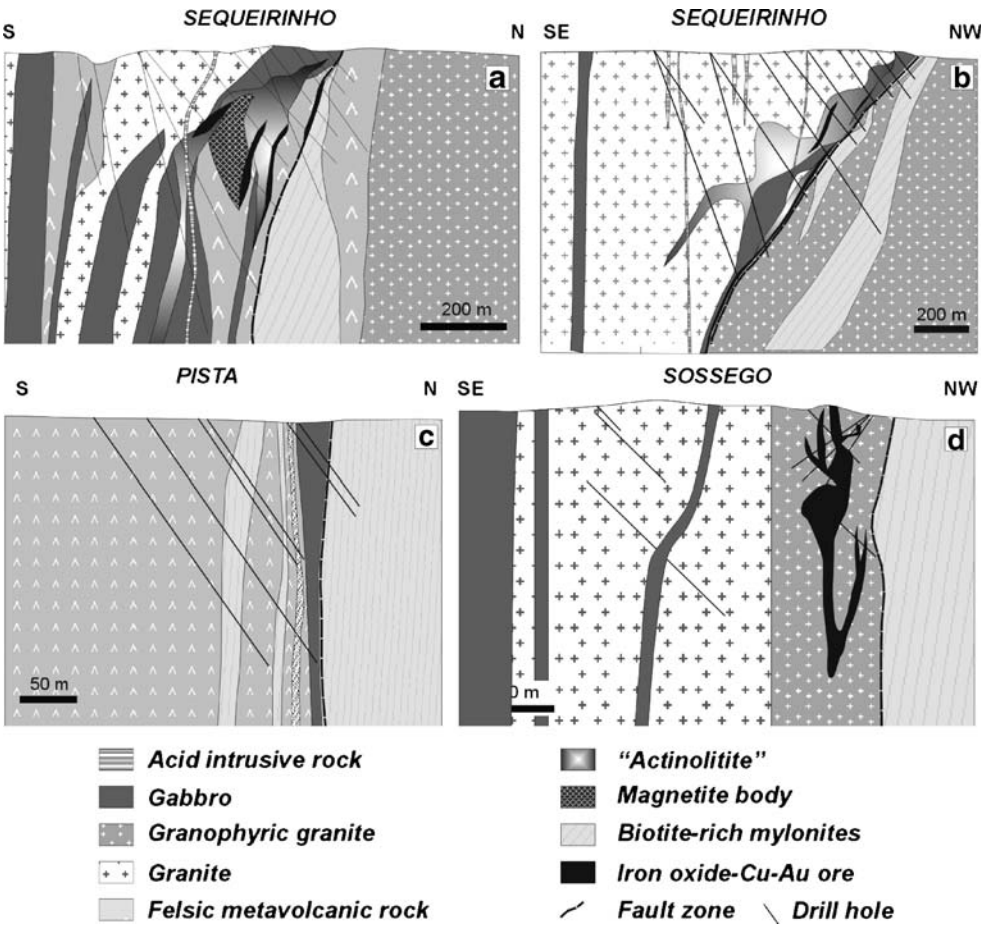

Fig. 3 Simplified cross-section of the Sequeirinho, Sossego, and Pista orebodies of the Sossego IOCG deposit (Companhia Vale do Rio Doce)

biotite in a very fine-grained quartz-feldspar matrix. Though generally unaltered, these dikes locally contain both magnetite and fine-grained disseminated chalcopyrite (Carvalho et al. 2005) suggesting that they were present during hydrothermal alteration and mineralization.

Hydrothermal alteration and mineralization

Though the type and intensity of alteration and mineralization varies among the different orebodies in the Sossego deposit, a consistent paragenetic sequence of alteration and

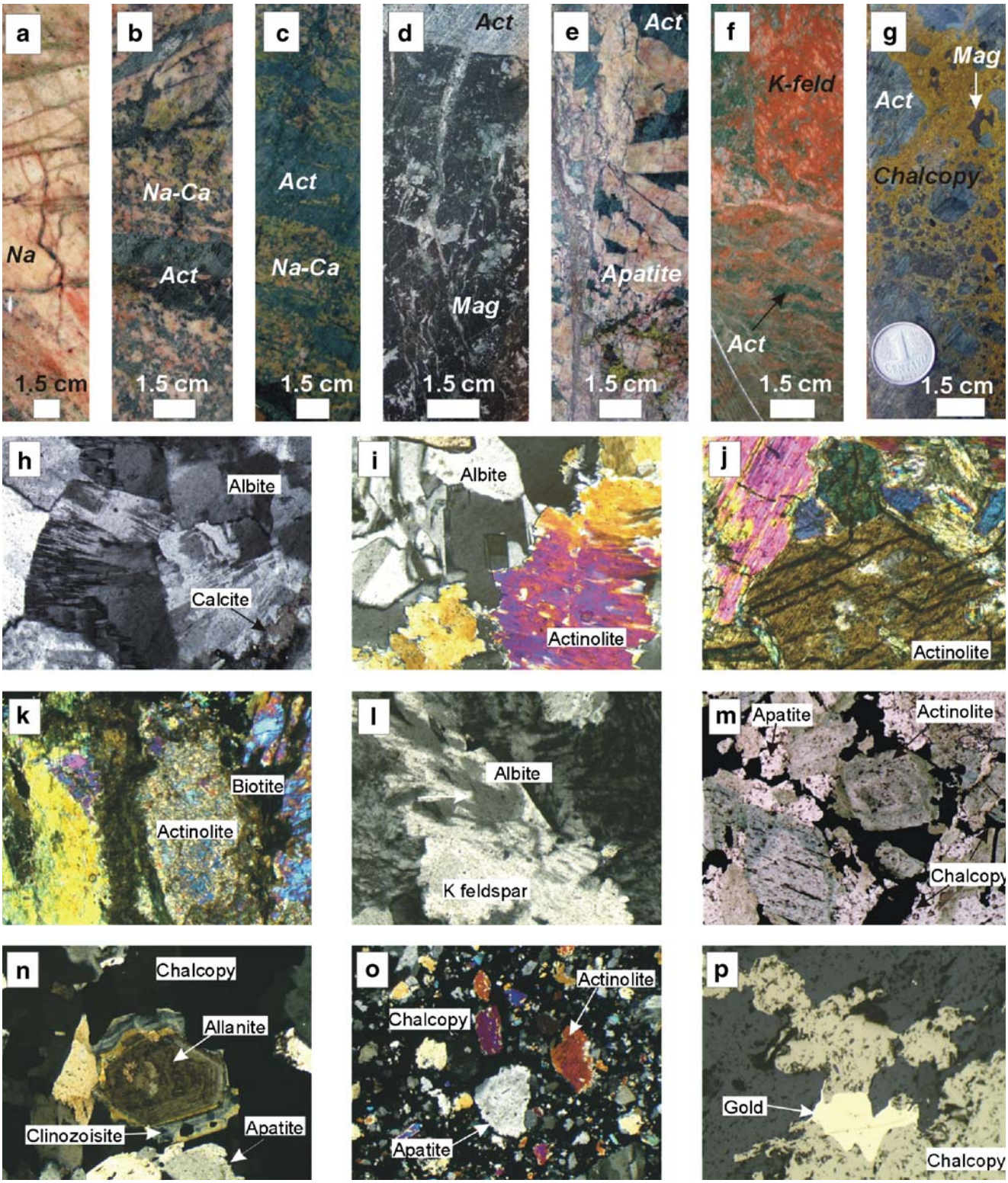

mineralization can be discerned. Sodic alteration, characterized by replacive to vein-controlled albitization, is prevalent in orebodies at the western portion of the deposit (Pista and Sequeirinho). A sodic–calcic alteration assemblage dominated by actinolite and albite occurs in all the orebodies at Sossego. Massive magnetite bodies occur with this alteration assemblage. This alteration assemblage cuts and replaces sodic alteration assemblages at Pista and Sequerinho. The sodic–calcic event was followed by potassic alteration and chloritization, which is best developed in the Sossego and Curral orebodies. Potassic alteration characterized by potassium feldspar, biotite, magnetite, and quartz is spatially associated with sulfide mineralized zones. The potassic alteration event appears to have occurred during a transition from ductile to brittle deformation. Sulfide mineralization was late. It generally cuts potassic alteration assemblages and is associated with renewed calcic alteration with predominance of epidote and very late hydrolytic alteration characterized by sericite–quartz–hematite–calcite.

Most mineralized zones at Sossego occur within breccia bodies that contain clasts of hydrothermally altered wall-rock in a matrix of sulfides, mainly chalcopyrite, and late alteration minerals.

Sequeirinho–Pista–Baiano orebodies

The Sequeirinho orebody (Figs. 3a,b, 4, and 5) is hosted by felsic metavolcanic rocks, granite, and gabbro and contains the largest portion of the reserves at Sossego. The Pista and Baiano orebodies represent extensions of the Sequeirinho to the west and east, respectively. The Pista orebody (Figs. 2 and 3c) is hosted predominantly by felsic metavolcanic rocks (Fig. 6) that contain lenses of metamorphosed ultramafic rocks (Fig. 6b); this metavolcanic sequence is cut by gabbro dikes. The Baiano orebody is hosted primarily within gabbro (Fig. 6i). These host rocks were strongly affected by both early sodic and later sodic–calcic alteration. The Sequeirinho orebody contains bodies of replacive magnetite associated with sodic–calcic alteration. The magnetite bodies are cut by relatively narrow zones of potassic alteration that form the locus for later structurally controlled, subvertical, breccia-hosted copper–gold mineralization.

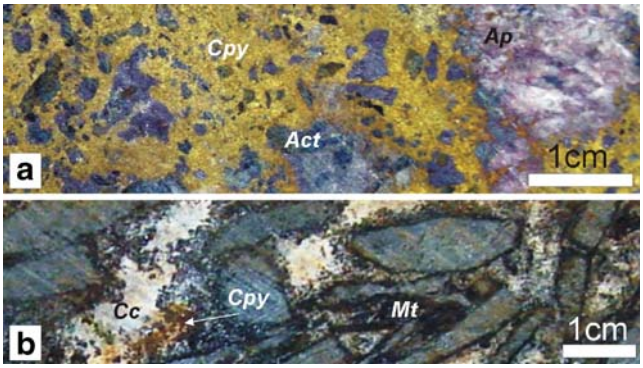

Fig. 5 Ore breccias in the Sequeirinho (**a**) and Sossego (**b**) orebodies. **a** Chalcopyrite associated with apatite, actinolitite, and magnetite fragments; **b** clast supported breccia with K altered and chloritized fragments of granophyric granite with magnetite rims within a calcite–quartz–chalcopyrite-rich matrix

Sodic alteration

Sodic alteration is recognized in all rock types south of the fault separating the block hosting the Sequeirinho–Pista–Baiano orebodies from the block hosting the Sossego–Curral orebodies (Fig. 2a). The sodic alteration was strongly controlled by the regional ductile–brittle shear zones, especially in the Pista area. This alteration was commonly pervasive, but fracture-controlled veinlets of albite also occur.

The sodic alteration resulted in precipitation of fine- to medium-grained albite that contains extremely fine-grained hematite inclusions that impart a pink color to the altered rocks (Figs. 4a and 6c). Albite commonly has chessboard texture and exhibits undulose extinction, grain boundary granulation, and recrystallization, indicating that albite formed before and during deformation.

Scapolite and tourmaline are conspicuous within the sodic assemblage in the felsic metavolcanic rocks, which are predominant at Pista. Mylonitized metavolcanic rocks affected by sodic alteration exhibit alternating bands of albite, tourmaline, or scapolite (Fig. 6d,j). Sodically altered rocks are cut by shear zones. These structural zones display

◀ **Fig. 4** Characteristic features of hydrothermal alteration and ore from the Sequeirinho body. **a** granite affected by pervasive Na-alteration characterized mainly by pinkish albite; **b** Na-altered granite affected by Na–Ca alteration represented by actinolite, epidote, carbonate, and titanite; **c** Na–Ca altered granite cut by actinolite veins; **d** strongly Na–Ca altered rock composed of actinolite and magnetite, which are locally fractured and cut by calcite veinlets; **e** coarse-grained apatite crystals associated with actinolite and cut by chalcopyrite veinlets; **f** felsic metavolcanic rock replaced by actinolite (Na–Ca alteration) and later potassic alteration with K feldspar; **g** sequeirinho ore breccia containing clasts of actinolite and apatite in a chalcopyrite-rich matrix; **h** hydrothermal albite that pervasively replaced the Sequeirinho host rocks. Plane polarized light; width of field=1.25 mm; **i** Na–Ca alteration assemblage of albite, actinolite (+ titanite, epidote, calcite). Plane polarized light; width of field=1.25 mm. **j** Intergrown actinolite crystals in actinolitite. Plane polarized light; width of field=4 mm; **k** actinolite replaced by biotite along fractures. Plane polarized light; width of field=0.7 mm. **l** albite replaced by K feldspar associated with potassic alteration. Plane polarized light; width of field=0.7 mm; **m** zoned actinolite crystals and apatite (Na–Ca assemblage) cut by chalcopyrite in the matrix of breccia ore. Plane polarized light; width of field is 4 mm; **n** euhedral allanite with epitaxial overgrowth of clinozoisite overgrown by chalcopyrite. Plane polarized light; width of field=1.25 mm; **o** Sequeirinho ore with chalcopyrite, that cuts and replaces preexisting actinolite and apatite. Plane polarized light; width of field=4 mm; **p** gold inclusion in chalcopyrite in the Sequeirinho ore. Reflected light; width of field=0.7 mm

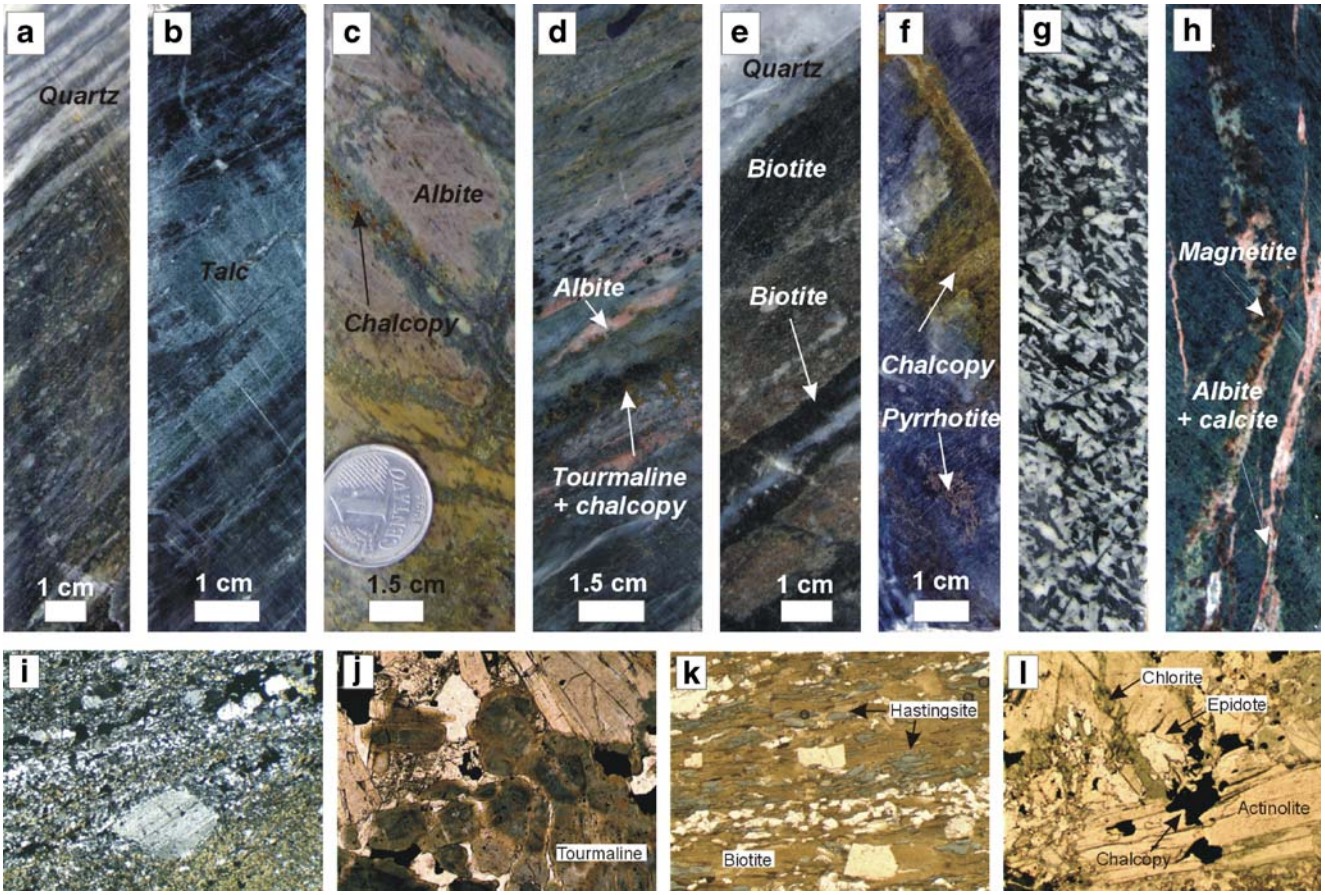

Fig. 6 Characteristic features of the hydrothermal alteration and ore from the Pista (**a**–**f** and **i**–**l**) and Baiano (**g**–**h**) orebodies. **a** Weakly altered felsic metavolcanic rock affected by mylonitization and silicification; **b** mylonitized metamorphosed ultramafic rock with talc bands; **c** felsic metavolcanic rock that has undergone pervasive Na alteration represented by pinkish albite and later, fracture-controlled Ca alteration with actinolite, calcite, chlorite, and chalcopyrite; **d** felsic metavolcanic rock replaced by an early Na alteration assemblage of albite, scapolite, tourmaline. The rock was later affected by silicification associated with mylonitization. Late chalcopyrite occurs as fracture infillings in tourmaline-rich zones; **e** potassically altered felsic metavolcanic rock cut by quartz veins with biotite-rich selvages; **f** silicified felsic metavolcanic rock cut by chalcopyrite veinlets; **g** least-altered gabbro with ophitic texture composed of pyroxene and plagioclase; **h** chloritized gabbro cut by magnetite and albite-calcite veinlets; **i**. weakly altered felsic metavolcanic rock affected by mylonitization. Plane polarized light; width of field is 2.4 mm; **j** tourmaline crystals in sodically altered felsic metavolcanic rock. Plane polarized light; width of field is 4 mm; **k** felsic metavolcanic rock replaced by biotite (potassic alteration) and hastingsite-tourmaline. Plane polarized light; width of field is 2.4 mm; **l** Chalcopyrite associated with chlorite in late Ca vein (actinolite, epidote, apatite, quartz) cutting felsic metavolcanic rock. Plane polarized light; width of field is 1.25 mm

a range of textures from well-developed mylonitic fabrics to more brittle, fracture zones. Silicification predominates in the more ductile zones, whereas epidote is most common as vein fillings in fractures.

Sodic–calcic alteration

Regional fracture-controlled sodic–calcic alteration is recognized to south of the Sequeirinho orebody, affecting all host rock types and also migmatites and gneiss of the Xingu Complex (Fig. 2). Towards the mineralized zones, fracture-controlled sodic–calcic alteration becomes pervasive in rocks with a mylonitic fabric. This alteration assemblage cuts and replaces albite-altered rocks (Fig. 4b–d). Sodic–calcic alteration assemblages are dominated by actinolite and albite and commonly contain accessory magnetite, calcite, epidote, quartz, titanite, allanite, and thorianite. At Sequeirinho, this alteration is associated with bodies of replacive magnetite.

Sodic–calcic alteration is best developed in gabbroic host rocks. Adjacent to contacts between the gabbros and metavolcanic rocks/granite, assemblages of Cl-rich ferro-edenite/hastingsite, albite and magnetite are present. Pervasive sodic–calcic alteration grades into zones of massive, coarse-grained (up to 3 cm long) actinolite crystals intergrown with magnetite (Fig. 4d). This rock type, termed "actinolitite", forms zones up to 80 m wide around massive magnetite bodies.

Massive magnetite forms subvertical bodies parallel to the fault bounding the orebody. These bodies can reach thicknesses of >50 m and appear to replace gabbro, granite, and felsic metavolcanic rocks. They are composed of

coarse-grained, euhedral to subhedral magnetite. The magnetite is locally intergrown with and locally cut by apatite. Veins of coarse reddish apatite with crystals up to 10 cm in length (Fig. 4e) cut magnetite and the surrounding coarse-grained actinolite. Both magnetite and actinolitite are cut by brittle veins containing epidote or epidote–calcite–hematite–quartz assemblages.

Potassic alteration

Potassic alteration overprints both sodic and sodic–calcic alteration assemblages. This alteration type is poorly developed in the Sequeirinho orebody. It is best developed in felsic metavolcanic rocks at Pista.

Potassic alteration zones are represented by two different assemblages. The first forms narrow zones controlled by steep, vein-like structures and contains K feldspar, Cl-rich biotite, quartz, magnetite, and minor allanite, thorianite, and chalcopyrite. Hydrothermal potassium feldspar is conspicuous due to its intense red color (Fig. 4f), which results from inclusion of numerous small grains of hematite. Hydrothermal albite is mantled and replaced by potassium feldspar and may display fractures filled with potassium feldspar. Actinolite is converted to biotite in potassically altered zones (Fig. 4k,l). Sodic–calcic altered gabbro bodies display replacement of hydrothermal hastingsite by biotite and pyrrhotite. In the Pista orebody, the felsic metavolcanic rocks commonly display fractures filled with a biotite–potassium feldspar–quartz assemblage that have biotite selvages.

A distinct potassic alteration assemblage represented by biotite ± hastingsite–tourmaline–scapolite (Fig. 6e,k) also pervasively replaced mylonitized metavolcanic rocks in the Pista orebody. This alteration type is similar to that found in the footwall zones of the Sequeirinho and Sossego orebodies (Fig. 2).

Chloritization

Fracture controlled potassic alteration commonly exhibits chlorite-rich halos that grade outward to a calcite–epidote association, particularly within the felsic metavolcanic rocks of the Pista orebody. These zones also contain minor titanite, rutile, apatite, and albite as well as minor chalcopyrite.

Copper–gold mineralization

The majority of the sulfide mineralization was concentrated within steeply dipping bodies that contain fragments of massive magnetite and actinolitite within a matrix of hydrothermal minerals including sulfides (Figs. 4g and 5a).

The earliest mineral assemblage forming the breccia matrix consists of coarse-grained actinolite/ferroactinolite, Cl–apatite, and magnetite. Amphibole from this association is euhedral and strongly zoned (Fig. 4m), commonly with darker rims, differing from that associated with Na–Ca alteration and actinolitite. Later, and more common, minerals comprising the breccia matrix include epidote, chlorite, quartz, calcite, and sulfides.

Paragenetically, early minerals within the breccia matrix commonly are altered along grain boundaries and fractures. Actinolite is variably replaced by chlorite or epidote. Magnetite has reaction rims of hematite and quartz, as well as titanite, ilmenite, and rutile veinlets. Apatite is overgrown by fine-grained monazite and REE-rich epidote, chlorite, and chalcedony. Altered zones in apatite are evidenced by yellowish cathodoluminescence (CL) that is different from the bright green CL observed in unaltered apatite. These features possibly reflect interaction of preexisting minerals with the mineralizing fluids. Textures in the breccias and the fracture control of later alteration minerals such as chlorite and epidote indicate that mineralization occurred in a brittle structural regime.

Sulfide mineralization was coincident with a late alteration association containing epidote group minerals, primarily epidote and Ce–allanite, chlorite, and lesser calcite and quartz. Epidote forms zoned, euhedral crystals occasionally replacing actinolite (Fig. 4m). Ce–allanite occurs as coarse-grained crystals with fine-grained thorianite inclusions and epitaxial overgrowths of clinozoisite or epidote (Fig. 4n). Pyrite is the dominant early sulfide and occurs as subidiomorphic crystals. It is overgrown and replaced by chalcopyrite (Fig. 4o), which is the predominant sulfide phase comprising >85% of the ore. Chalcopyrite also replaces magnetite. Siegenite is commonly intergrown with chalcopyrite and commonly is cut and replaced by millerite. Gold (with 10 to 15% Ag; Fig. 4p), Pd–melonite, sphalerite, galena, cassiterite, and hessite represent minor phases and occur as fine-grained inclusions in chalcopyrite. Though most sulfides are undeformed, zones with highly strained chalcopyrite are observed indicating continued deformation during mineralization.

In the Pista orebody, sulfide mineralization occurred after a late calcic alteration that formed veins of actinolite–magnetite–epidote–apatite–calcite–(pyrrhotite) (Fig. 6l). Sulfides are intergrown with calcite, chlorite, epidote, titanite, and allanite; a similar assemblage is present at Sequeirinho. Sulfide minerals occur as disseminations along mylonitic fabrics (Fig. 6f) and within steeply dipping veins and stockwork breccias. Both veins and the matrix of ore breccias contain an assemblage of chalcopyrite–(pyrrhotite–pyrite–molybdenite); minor sphalerite, siegenite, and millerite are also present. The mineralized zones typically contain iron–titanium oxides. Disseminated chalcopyrite and pyrite also occur within strongly silicified zones and associated with a late hydrolytic assemblage of

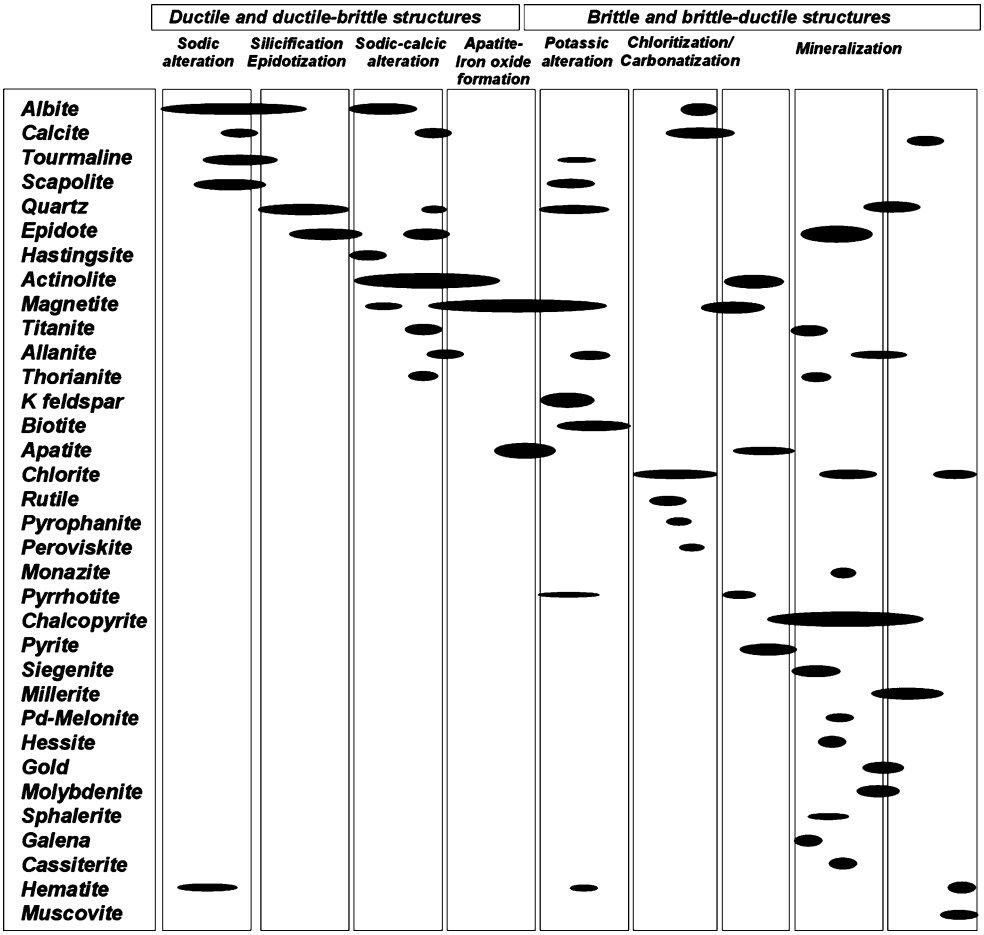

Fig. 7 Mineral associations and paragenetic sequence of hydrothermal alteration and mineralization in the Sequeirinho–Pista–Baiano orebodies

muscovite, chlorite, calcite, quartz, and hematite. In the Baiano orebody, calcite–chlorite–epidote–chalcopyrite–(albite) veins crosscutting chloritized gabbro (Fig. 6h) form the majority of the potentially economic mineralization. Paragenetic associations in the Sequeirinho–Pista–Baiano orebodies are presented in Fig. 7.

Sossego–Curral orebodies

The Sossego orebody and its SW extension, the Curral orebody, occur to the northeast of the Sequeirinho orebody and are separated from it by a major, generally E–W trending high angle fault. The Sossego–Curral orebodies are restricted largely to granophyric granite host rocks (Fig. 3d), though some mineralized zones also occur within granite and felsic metavolcanic rocks. The Sossego–Curral orebodies display a similar alteration sequence to that at Sequeirinho but have better developed potassic and chloritic alteration assemblages and contain a late hydrolytic alteration assemblage. Sulfides at Sossego–Curral are largely restricted to subvertical breccia pipes that contain open vugs. The dominance of potassic alteration and chloritization and the presence of hydrolytic alteration assemblages, together with the evidence for open space

Fig. 8 Characteristic features of hydrothermal alteration and ore from the Sossego–Curral orebodies. **a** Least-altered granophyric granite; **b** pervasive Na alteration of granophyric granite with late chlorite veins; **c** granophyric granite cut by veins of biotite, chlorite, magnetite, calcite, and chalcopyrite; **d** Potassically altered granophyric granite with red potassium feldspar cut by later veins of actinolite and chlorite (late Na–Ca alteration); **e** mineralized breccia with calcite-rich matrix (+ chalcopyrite, quartz, apatite, actinolite, chlorite) enclosing fragments of granophyric granite; **f** late calcite, quartz, apatite cutting granophyric granite; **g** quartz and feldspar intergrowth in weakly-altered granophyric granite. Plane polarized light; width of field= 0.7 mm; **h** chessboard albite that occurs replacing the granophyric granite. Plane polarized light; width of field=2.4 mm; **i** early hydrothermal albite replaced by K feldspar (potassic alteration). Plane polarized light; width of field=0.7 mm; **j** potassic alteration assemblage of biotite, K feldspar and magnetite in granophyric granite. Plane polarized light; width of field=1.25 mm; **k** fracture-controlled chloritization with associated rutile, titanite, and calcite. Plane polarized light; width of field=1.25 mm; **l** K feldspar replaced by calcite in mineralized rock. Plane polarized light; width of field= 0.7 mm; **m** apatite, calcite, muscovite, and quartz in the matrix of the mineralized breccia. Plane polarized light; width of field= 1.25 mm; **n** euhedral quartz, calcite, zoned epidote, and chlorite in the matrix of mineralized breccia. Plane polarized light; width of field is 4 mm; **o** magnetite, pyrite, chalcopyrite, and siegenite forming the matrix of a mineralized breccia. Reflected light; width of field=1.25 mm

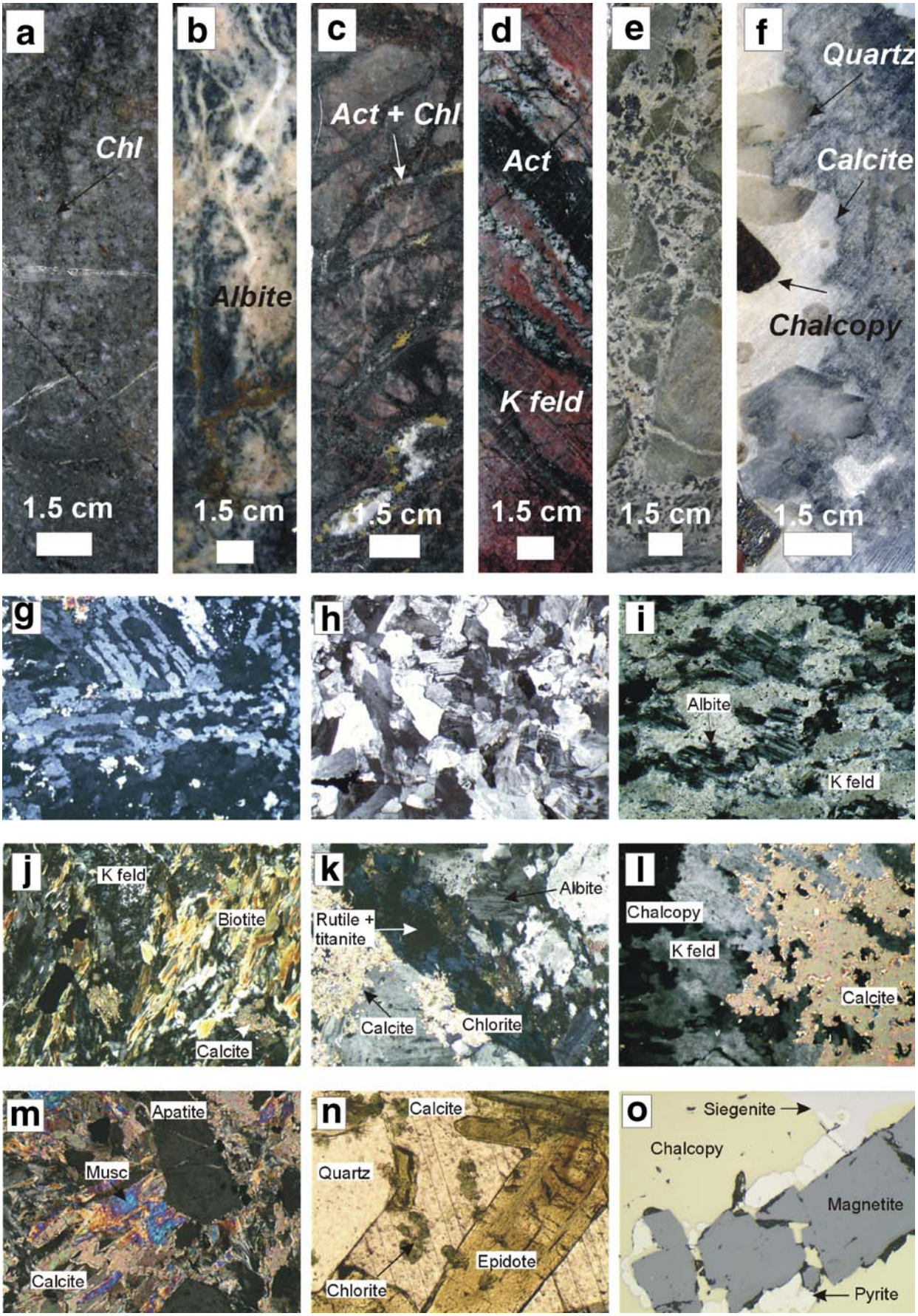
a
Chl
1.5 cm
b
Albite
1.5 cm
c
Act + Chl
1.5 cm
d
Act
K feld
1.5 cm
e
1.5 cm
f
Quartz
Calcite
Chalcopy
1.5 cm
g
h
i
Albite
K feld
j
K feld
Biotite
Calcite
k
Albite
Rutile + titanite
Calcite
Chlorite
l
Chalcopy
K feld
Calcite
m
Apatite
Musc
Calcite
n
Calcite
Quartz
Epidote
Chlorite
o
Siegenite
Chalcopy
Magnetite
Pyrite

filling of porosity in the breccias suggest that Sossego–Curral represents the structurally highest portions of the Sossego ore system. This alteration zoning is similar to that observed in the Candelaria–Punta del Cobre, Chile IOCG system (Marschik and Fontboté 2001).

Sodic and sodic–calcic alteration

Early sodic and sodic–calcic alteration at Sossego–Curral have been largely overprinted by later potassic assemblages. Albite veinlets (Fig. 8b,k) related to early sodic alteration are observed cutting granophyric granite, granite, and felsic metavolcanic rocks outboard of the mineralized zone. Within the zone of potassic alteration, some remnants of sodic assemblages are preserved as massive albitite replaced by potassium feldspar. Like the Sequeirinho–Pista–Baiano ore zones, the Sossego–Curral orebodies contain zones of albite that are cut and replaced by silicification along high-angle shear zones.

Rare clasts of actinolite–albite–magnetite–apatite altered rock similar to that from the sodic–calcic zone of Sequeirinho, are locally present within ore breccias. The paucity of calcic–sodic alteration in the Sossego–Curral orebodies may be due in part to the lack of the most favorable gabbroic host rocks. However, it is also probable that the Sossego–Curral zone was located higher in the system and was not subjected to as intense sodic and sodic–calcic alteration.

Potassic alteration

Potassic alteration is well developed in the Sossego and Curral orebodies. It occurs in replacement zones close to mineralized zones (Fig. 8d,i,j) and is characterized by the assemblage Cl-rich biotite–potassium feldspar–quartz ± magnetite. Potassium feldspar is mainly coarse-grained and generally displays a cloudy appearance in thin section due to numerous tiny inclusions of fine-grained hematite, quartz, and calcite, and minor barite, uraninite, galena, sphalerite, pyrrhotite, or magnetite.

Potassic alteration varies from pervasive near the mineralized zones to vein controlled further from well-mineralized areas. Potassium feldspar mantles albite or occurs as fracture infilling in albite and commonly contains minor chalcopyrite associated. The most intense potassic alteration zones are dominated by pervasive biotitization with associated magnetite, which grade outwards to chlorite–magnetite enriched zones.

Chloritization and carbonatization

Potassically altered rocks at Sossego–Curral, like those elsewhere in the Sossego system are cut by chlorite veins and zones of chlorite replacement. This alteration type is well developed at Sossego–Curral, where it forms a broad envelope around the area of potassic alteration. This style of alteration has resulted in the formation of (1) veinlets of chlorite and calcite with subordinate quartz, titanite, rutile, and magnetite (Fig. 8k); and (2) pervasively chloritized zones in which biotite was converted to Fe-rich chlorite. Calcite veins increase in intensity near mineralized zones. These veins contain minor apatite, albite, epidote, and muscovite, in addition to calcite and chlorite.

Copper–gold mineralization and late hydrolytic alteration

Mineralization at Sossego–Curral occurs within vein and breccia bodies (Figs. 5b, 8e–g). In plan view, the breccia bodies are circular in shape and their contacts with host rocks are sharp, although marked by occurrence of mineralized vein networks related to radiating fracture patterns. The breccias are predominantly clast-supported (Fig. 5b), but matrix-supported breccias are also recognized. Clasts are locally derived, mainly from the host granophyric granite. The clasts are angular to subrounded and range from <0.5 to >10 cm in diameter. Commonly, clasts were strongly affected by potassic alteration (biotite–magnetite–quartz) before brecciation and are rimmed by magnetite.

Veins and breccias at Sossego–Curral were initially filled with an assemblage of magnetite–actinolite–biotite–apatite–calcite–epidote with minor sulfides (pyrite–chalcopyrite). This assemblage represents the main infilling stage of the veins. These minerals appear to have grown into open space as evidenced by euhedral magnetite that is overgrown by coarse-grained, euhedral, zoned actinolite. Within breccia matrix, amphibole is euhedral and strongly zoned, similar to that found in the Sequeirinho breccias. Apatite in these veins and breccias is pinkish and chlorine-rich. Calcite (I) commonly displays undulose extinction and a homogeneous red cathodoluminescence.

The early assemblage is overprinted by an assemblage of sulfides, quartz, calcite (II), Fe–chlorite, epidote, late apatite, and muscovite (Fig. 8m,n), which represent the main mineralization stage at Sossego–Curral. These minerals are commonly coarse-grained with equant quartz and calcite crystals up to 1 cm in length; coarse-grained apatite and chalcopyrite are also present (Fig. 8f). Minerals from this stage do not exhibit evidence of deformation. Breccias with a chalcopyrite-rich matrix, similar to those from the Sequeirinho orebody, also occur in central zones of the breccia bodies. Sulfides are chalcopyrite and pyrite, with lesser siegenite (Fig. 8o), millerite, hessite, Pd–melonite, and molybdenite (Fig. 9). Gold occurs as inclusions within chalcopyrite. Minor cassiterite is also present.

The latest stage of alteration at Sossego–Curral is represented by an assemblage of sericite–hematite–quartz–

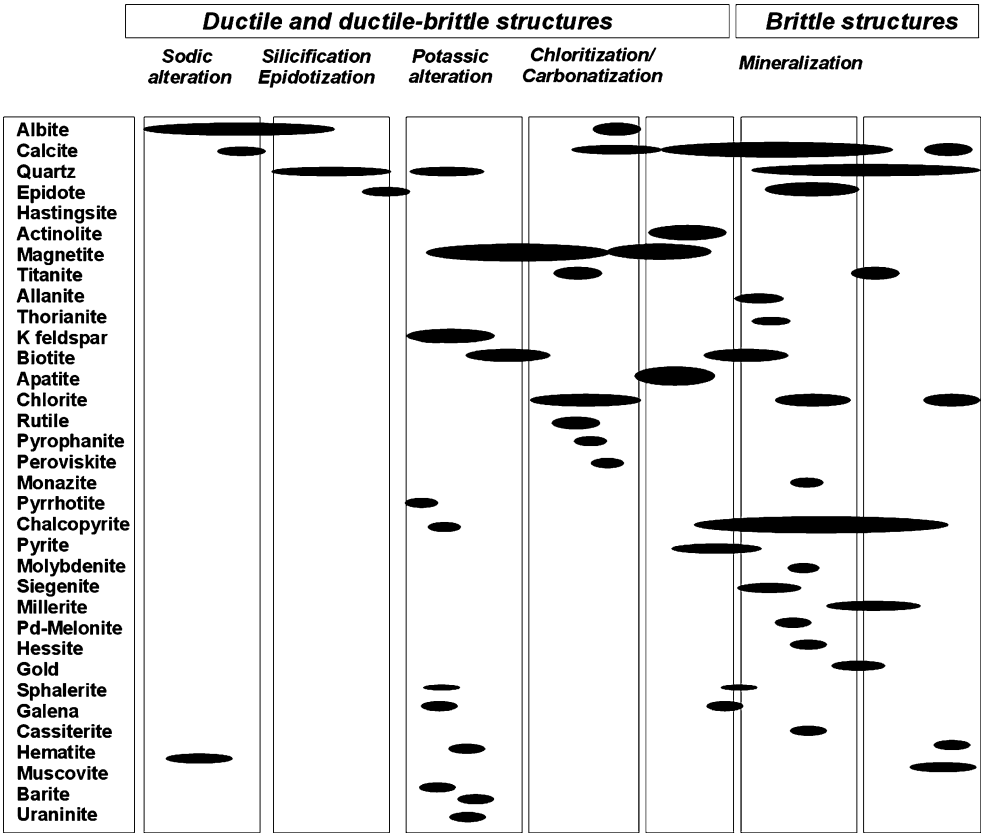

Fig. 9 Mineral associations and paragenetic sequence of hydrothermal alteration and mineralization in the Sossego–Curral orebody

chlorite–(calcite III) that locally cuts mineralized breccias. Such zones are generally poorly mineralized and appear to represent a late, high-level zone of hydrolytic alteration. The paragenetic evolution at Sossego–Curral is presented in Fig. 9.

Stable isotopes

Oxygen isotopes

Oxygen isotope studies were carried out on albite ($\delta^{18}O_{VSMOW}$=5.4 to 7.8‰), K feldspar (5.1‰), actinolite (4.8 to 5.9‰), magnetite (−0.8 to 1.8‰), apatite (0.9 to 15.2‰), epidote (0.0 to 0.3‰), chlorite (−1.8‰), quartz (5.9 to 9.8‰), and calcite (4.8 to 18.3‰), representing several different alteration stages of the Sossego hydrothermal system (Tables 3, 4, and 5). Apatite has the widest isotopic variation, reaching a high of 15.2‰. Calcite from mineralized breccias of the Sossego–Curral and Sequeirinho orebodies has narrow isotopic variation ($\delta^{18}O$ values=6.8±1.7; n=30). However, late calcite from veins that crosscut magnetite ± albite ± actinolite–replaced gabbro of the Sequeirinho and Baiano orebodies show wider ranges ($\delta^{18}O$=11.7±6.6‰; n=7).

Temperature conditions

Temperatures were calculated for several mineral pairs using the oxygen isotope fractionation factors of Zheng (1991, 1993a,b, 1994, 1996). Petrographic criteria were used to identify coeval mineral phases with evidences of textural equilibrium within the same microstructural domain. Minerals showing retrograde alteration were not chosen for thermometry. In the Sequeirinho orebody, an albite–actinolite pair give an isotopic temperature of 500± 25°C for early Na–Ca alteration. Slightly higher temperatures (550±25°C) were obtained from actinolite–magnetite pairs associated with the actinolitite or massive magnetite bodies (Table 2). Calcite–epidote and quartz–epidote pairs associated with late calcic alteration within mineralized breccias give temperatures of 230±25°C for the mineralization stage.

In the Sossego orebody, calcite–actinolite pairs give an isotopic temperature of 460±25°C for early vein or breccia formation. Temperature for the main mineralization stage estimated from quartz–calcite and calcite–apatite is 275± 25°C. In the Baiano orebody, magnetite and calcite associated with early gabbro-hosted veins yielded temperature of 410±25°C, whereas the isotopic temperature for epidote–calcite from late mineralized veins is 190±25°C.

Table 2 Calculated oxygen isotopic temperatures for hydrothermal alteration stages and mineralization in the Sossego deposit and comparison with conditions estimated using geothermometers based on mineral chemistry

		Oxygen isotopes[a]	Mineral chemistry[b]
Sequeirinho	Na–Ca alteration	500±25°C (Ab–Act pair)	500±30°C at 1.5 kbar (TWQ software, Berman 1991) 540±40°C (Plag–Amp geothermometer of Holland and Blundy 1994)
	Actinolitite	517°C (Act–Mag pair) 550°C (Act–Mag pair) 574°C (Act–Mag pair) Mean=550±25°C	
	Ore	253°C (Qtz–Ep) 208°C (Cal–Ep) Mean=230±25°C	255±30°C (chlorite geothermometer of Cathelineau and Nieva 1985)
Baiano	Early vein infilling	410±25°C (Act–Mag pair)	
	Late vein infilling	190±25°C (Cal–Ep pair)	
Sossego	Early vein infilling	460±25°C (Cal–Act pair)	
	Late vein infilling	302°C (Qtz–Cal pair) 253°C (Cal–Ep pair) Mean=275±25°C	210±40°C (chlorite geothermometer of Cathelineau and Nieva 1985)

Temperatures were calculated using the oxygen isotope fractionation factors of Zheng (1991, 1993a,b, 1994, 1996).
Ab albite, *Act* actinolite, *Ap* apatite, *Cal* calcite, *Ep* epidote, *Mag* magnetite, *Qtz* quartz
[a] This study
[b] Monteiro et al. (2004a)

Table 3 Oxygen isotope composition of silicates, oxides, and phosphate of the Sequeirinho and Baiano orebodies from the Sossego IOCG deposit

Sample	Hydrothermal alteration	Minerals		T°C[a]	$\delta^{18}O_{fluid}$ (‰)[b]
Sequeirinho orebody					
352/205.80	Na alteration	(Ab) 5.4		450±50	3.6±0.6
SOS 2C	Silicification	(Qtz) 9.3		400±50	4.8±0.9
99/603.72	Silicification	(Qtz) 9.8		400±50	5.2±1.0
SOS 10A	Regional Na–Ca alteration	(Ab) 6.3	(Act) 5.1	500±25	5.9±1.1
280/488.67	Na–Ca alteration	(Ab) 7.8	(Act) 4.8	500±25	6.0±0.8
259/264.60	Actinolitite		(Act) 5.9	550±25	7.7±0.1
SOS 39K	Actinolitite	(Mag) −0.1	(Act) 5.2	550±25	6.7±0.2
352/122.80	Actinolitite	(Mag) −0.1	(Act) 4.9	550±25	6.7±0.2
SOS 39L	Actinolitite	(Mag) 0.0	(Act) 4.8	550±25	6.8±0.2
SOS 39D	Iron oxide stage	(Mag) −0.7		550±25	6.1±0.2
22/273.78	Iron oxide stage	(Mag) −0.2		550±25	6.6±0.2
280/421.40	Iron oxide stage	(Mag) −0.1		550±25	6.7±0.2
22/312.67	Breccia infilling	(Act) 2.8		400±50	3.4±0.4
259/264.60	Breccia infilling	(Ap) 4.0		400±50	4.0±0.4
259/267.15	Breccia infilling	(Ap) 1.6		400±50	1.6±0.4
99/292.25	Breccia infilling	(Ap) 0.9		400±50	0.9±0.5
SOS 38C	Mineralization (ore breccia)	(Ep) 0.0		230±25	−2.9±0.8
SOS 39 K	Mineralization (ore breccia)	(Qtz) 5.9		230±25	−4.1±1.3
SOS 39L	Mineralization (ore breccia)	(Qtz) 6.0		230±25	−4.0±1.3
Baiano orebody					
279/126.68	Early vein/breccia filling	(Mag) 0.9		400±25	8.7±0.2
279/154.08	Early vein/breccia filling	(Mag) −0.2		400±25	7.6±0.2
279/126.68	Late vein filling	(Ep) 0.6		200±25	−4.1±1.2
279/154.08	Late vein filling	(Ep) 0.0		200±25	−4.2±1.1

[a] Temperature intervals represent calculated oxygen isotope temperatures for mineral pairs and conditions estimated from geothermobarometry. See text for discussions.
[b] Oxygen isotope fractionations: magnetite–H_2O (Zheng 1991); albite–H_2O, quartz–H_2O (Zheng 1993a); actinolite–H_2O; epidote–H_2O (Zheng 1993b); apatite–H_2O (Zheng 1996).

With few exceptions (e.g., selected apatite–actinolite, calcite–apatite, and calcite–actinolite pairs) the order of oxygen isotope partitioning of the different minerals conforms to the order of equilibrium partitioning and the isotopic temperatures are consistent with the results of other geothermometers for the Sossego deposit presented in Table 2. Thus, the isotopic data for these three orebodies suggest that temperature decreased markedly through the paragenesis.

Oxygen isotopic composition of the hydrothermal fluids

Oxygen isotope fractionation factors for magnetite–H_2O (Zheng 1991), albite–H_2O, K feldspar–H_2O, and quartz–H_2O (Zheng 1993a), actinolite–H_2O and epidote–H_2O (Zheng 1993b), chlorite–H_2O (Savin and Lee 1988), calcite–H_2O (Zheng 1994), and apatite–H_2O (Zheng 1996) were used to calculate the isotopic composition of coexisting water for the temperature ranges estimated for each alteration stage (Tables 3, 4, and 5).

For the Sequeirinho orebody (Table 3), $\delta^{18}O_{H_2O}$ values for fluids associated with Na alteration (450±50°C) is 3.6±0.6‰. Regional fracture-controlled $\delta^{18}O_{H_2O} = -1.8 \pm 3.4‰$ and pervasive Na–Ca alteration $\delta^{18}O_{H_2O} = 5.9 \pm 1.1‰$ at Sequeirinho are associated with slightly higher $\delta^{18}O_{H_2O}$ values at 500± 25°C. Fluids associated with silicification, which was broadly synchronous with the development of regional shear zones, have $\delta^{18}O_{H_2O}$ values of 4.8±0.8‰ at 400±50°C. Relatively high $\delta^{18}O_{H_2O}$ values are associated with actinolitite (7.2±0.6‰) and massive magnetite bodies (6.5±0.5‰) at Sequeirinho, both of which formed at the temperature of 550±25°C (Table 3).

The temperature of apatite formation is uncertain, but the relatively small fractionation between chlorapatite and H_2O (Zheng 1996), indicate lower $\delta^{18}O_{H_2O}$ values (2.4±2.0‰, at 400±5°C) for the fluid present during formation of this mineral. This might be consistent with the brittle deformation regime that is inferred for apatite formation, which would have allowed meteoric fluids access to the system. Alternatively, the ^{18}O-depleted compositions could reflect exchange between apatite and retrograde fluids, a phenomenon that is suggested by petrographic and cathodoluminescence evidence.

In the Sequeirinho ore breccia, early coarse-grained zoned actinolite formed from a fluid with $\delta^{18}O_{H_2O}$ of 3.4±0.4‰ (400±50°C). The calculated $\delta^{18}O_{H_2O}$ values for fluids in equilibrium with calcite (−0.4±2.3‰), epidote (−2.9±0.8‰), and quartz (−4.1±1.3‰), at 230±25°C, suggests a progressive influx of an ^{18}O-depleted fluid in the mineralization stage. Overall the Sequeirinho $\delta^{18}O_{H_2O}$ values appear to have decreased through time (Fig. 10).

For the Baiano orebody, a similar trend of decreasing $\delta^{18}O_{H_2O}$ from early veins with magnetite $\delta^{18}O_{H_2O} = 6.0 \pm 0.8‰$ to late epidote-bearing veins (−4.2±1.2‰, at 200±25°C) is observed (Table 3). Calculated $\delta^{18}O_{H_2O}$ values for vein calcite in gabbro span a wider variation range (5.6±8.6‰).

Table 4 Oxygen isotope composition of silicates, oxides, and phosphate of the Sossego–Curral orebodies from the Sossego IOCG deposit

Sample	Association	Minerals	T (°C)[a]	$\delta^{18}O_{fluid}$[b]
Sossego–Curral orebody				
Sos 802	K alteration	(K feld) 5.1	460±25	3.6±0.3
419/143.24	Vein/breccia filling	(Mag) 1.8	400±50	9.7±0.3
319/112.02	Vein/breccia filling	(Mag) −0.8	400±50	7.1±0.3
419/136.94	Vein/breccia filling	(Act) 5.3	400±50	6.4±0.4
319/152.92	Vein/breccia filling	(Act) 4.7	400±50	5.7±0.4
319/150.29	Vein/breccia filling	(Act) 4.4	400±50	5.4±0.4
319/113.92	Vein/breccia filling	(Act) 3.6	400±50	4.6±0.4
314/299.00	Vein/breccia filling	(Ap) 4.6	400±50	4.6±0.5
314/195.9	Vein/breccia filling	(Ap) 4.0	400±50	4.0±0.5
419/130.37	Vein/breccia filling	(Ap) 4.0	400±50	4.0±0.5
314/166.8	Vein/breccia filling	(Ap) 2.8	400±50	2.7±0.5
35/159.00	Vein/breccia filling	(Ap) 9.0	400±50	8.9±0.5
419/56.73	Vein/breccia filling	(Ap) 15.2	400±50	15.2±0.5
314/202.70	Mineralization	(Qtz) 7.7	275±25	0.4±1.0
319/113.92	Post mineralization	(Chl) −1.8	250±25	−5.5±1.0

[a] Temperature intervals represent calculated oxygen isotope temperatures for mineral pairs and conditions estimated from geothermobarometry. See text for discussions.

[b] Oxygen isotope fractionations: magnetite–H_2O (Zheng 1991); K feldspar–H_2O; quartz–H_2O (Zheng 1993a); actinolite–H_2O (Zheng 1993b); chlorite–H_2O (Savin and Lee 1988); apatite–H_2O (Zheng 1996).

Table 5 Oxygen and carbon isotope compositions of hydrothermal carbonates from veins and breccias of the Sossego IOCG deposit and calculated fluid compositions

Sample	Mineral	$\delta^{18}O$ (‰ SMOW)	$\delta^{13}C$ (‰ PDB)	T (°C)	$\delta^{18}O_{H_2O}$	$\delta^{13}C_{H^2CO^3(ap)}$
Sequeirinho (mineralized breccia) n=4						
SOS 22/224.36 (1)	Calcite	5.60	−4.77	230+25	0.1±1.1	−3.9±0.5
SOS 38C (1)	Calcite	5.07	−5.42	230+25	−1.5±1.1	−4.6±0.5
SOS12DSEQ (2)	Calcite	7.43	−6.44	230+25	0.8±1.1	−5.6±0.5
SOS12ESEQ (2)	Calcite	7.00	−5.68	230+25	0.4±1.1	−4.8±0.5
Sequeirinho/Baiano (veins in gabbro) n=6						
279/283.65 (1)	Calcite	4.99	−5.83	240+50	−1.0±2.0	−4.7±0.9
279/266.27 (1)	Calcite	5.66	−4.70	240+50	−0.4±2.0	−3.6±0.9
279/278.24 (1)	Calcite	5.53	−6.74	240+50	−0.5±2.0	−5.6±0.9
279/277.74 (1)	Calcite	6.99	−8.35	240+50	1.0±2.0	−7.2±0.9
279/283.28 (1)	Calcite	13.61	−5.69	240+50	7.6±2.0	−4.6±0.9
280/381.78 (1)	Calcite	18.26	−3.76	240+50	12.2±2.0	−2.7±0.9
Sossego–Curral (mineralized vein/breccia) n=26						
314/140.30 (2)	Calcite I	8.18	−5.49	400+50	6.2±0.8	−2.9±0.2
314/144.50 (2)	Calcite I	7.75	−5.36	400+50	5.8±0.8	−2.8±0.2
314/181.90 (2)	Calcite I	7.28	−5.89	400+50	5.3±0.8	−3.3±0.2
314/182.10 (2)	Calcite I	7.24	−5.90	400+50	5.3±0.8	−3.3±0.2
314/229.00 (2)	Calcite I	7.02	−6.03	400+50	5.0±0.8	−3.4±0.2
35/86.23 (1)	Calcite I	8.22	−6.03	400+50	6.2±0.8	−3.4±0.2
35/506.88 (1)	Calcite I	6.86	−6.68	400+50	4.9±0.8	−4.1±0.2
35/696.80 (1)	Calcite I	6.10	−7.64	400+50	4.1±0.8	−5.0±0.2
314/195.90 (1)	Calcite II	6.16	−5.78	275+25	1.3±0.9	−4.1±0.4
319/152.92 (1)	Calcite II	5.12	−5.01	275+25	0.3±0.9	−3.4±0.4
319/167.14 (1)	Calcite II	5.69	−5.82	275+25	0.8±0.9	−4.2±0.4
314/202.70 (1)	Calcite II	5.06	−4.81	275+25	0.2±0.9	−3.2±0.4
419/130.37 (1)	Calcite II	8.46	−5.90	275+25	3.6±0.9	−4.2±0.4
419/143.24 (1)	Calcite II	6.66	−5.04	275+25	1.8±0.9	−3.4±0.4
314/132.90 (2)	Calcite II	5.23	−5.73	275+25	0.4±0.9	−4.1±0.4
314/149.35 (2)	Calcite II	5.63	−5.87	275+25	0.8±0.9	−4.2±0.4
314/149.45 (2)	Calcite II	5.70	−5.83	275+25	0.8±0.9	−4.2±0.4
314/198.05 (2)	Calcite II	5.21	−5.35	275+25	0.4±0.9	−3.7±0.4
314/202.70 (2)	Calcite II	5.57	−4.73	275+25	0.7±0.9	−3.1±0.4
314/236.36 (2)	Calcite II	5.92	−5.77	275+25	1.1±0.9	−4.1±0.4
314/203.20 (2)	Calcite II	5.39	−5.35	275+25	0.5±0.9	−3.7±0.4
314/267.10 (2)	Calcite II	5.46	−6.03	275+25	0.6±0.9	−4.4±0.4
319/112.02 (2)	Calcite III	5.10	−4.67	250+25	−0.7±1.0	−3.4±0.4
319/113.92 (2)	Calcite III	4.81	−4.13	250+25	−1.0±1.0	−2.9±0.4
319/133.36 (2)	Calcite III	5.50	−5.03	250+25	−0.3±1.0	−3.8±0.4
319/152.92 (2)	Calcite III	5.63	−5.08	250+25	−0.1±1.0	−3.8±0.4

Temperature intervals represent calculated oxygen isotope temperatures for mineral pairs and conditions estimated from geothermobarometry and mineral stability fields. Oxygen mineral–water fractionation calculated from Zheng (1994) and carbon fractionation between calcite and CO_2 from Ohmoto and Rye (1979).
(1) This study, *(2)* Monteiro et al. (2004a; submitted).

For the Sossego orebody (Table 4), the $\delta^{18}O_{H_2O}$ value for the fluid associated with the potassic alteration (at 460±25°C) is 3.6±0.3‰, similar to the 3.6±0.6‰ value for the sodic alteration at Sequeirinho. Higher $\delta^{18}O_{H_2O}$ values were associated with early vein- and breccia-forming fluids associated with magnetite formation (8.4±1.6‰, at 400±50°C). Lower $\delta^{18}O_{H_2O}$ values were calculated for calcite I (5.2±1.9‰; Table 5) and actinolite (5.5±1.3‰) from this early infilling stage (Fig. 10), implying disequilibrium among these minerals and magnetite. This could be due to the decrease of $\delta^{18}O_{H_2O}$ of the evolving fluid or due to retrograde alteration of carbonate and amphibole. Fluids in equilibrium with apatite from the Sossego orebody had $\delta^{18}O_{H_2O}$ values of 3.7±1.5 (at 400±50°C) with some possible disequilibrium outliers suggesting values as high as 8.9±0.5‰ and 15.2±0.5‰.

The $\delta^{18}O_{H_2O}$ for the mineralization stage (275±25°C) at Sossego calculated from calcite II and quartz are 1.9±1.7‰

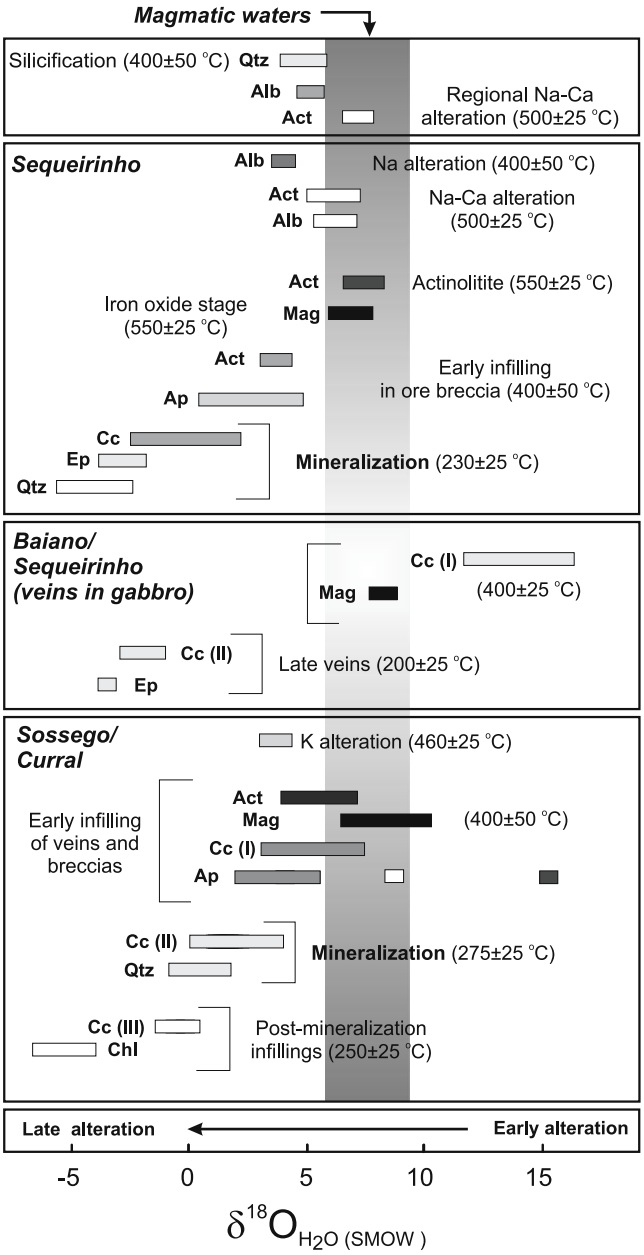

Fig. 10 Calculated oxygen isotopic compositions of the fluids associated with hydrothermal alteration and mineralization of the Sossego and Sequeirinho orebodies of the Sossego IOCG depositt. The shaded area represents the field of primary magmatic waters (Taylor 1968). Oxygen isotope fractionations: magnetite–H_2O (Zheng 1991); albite–H_2O, K feldspar–H_2O; quartz–H_2O (Zheng 1993a); actinolite–H_2O; epidote–H_2O; chlorite–H_2O (Savin and Lee 1988); calcite–H_2O (Zheng 1994); apatite–H_2O (Zheng 1996). *Ab* albite, *Act* actinolite, *Mag* magnetite, *Cal* calcite, *Ep* epidote, *Qtz* quartz, *Ap* apatite

and 0.4±1.0‰, respectively. Postmineralization calcite III and chlorite (250±25°C), related to hydrolytic alteration, gave lower values of −0.6±0.6 and −5.5±1.0‰, respectively (Tables 4 and 5).

Hydrogen isotopes

δD analyses were carried out on actinolite from regional Na–Ca alteration (δD=−76‰) and from Sequeirinho (−74 to −68‰) and Sossego (−93 to −70‰) hydrothermal alteration assemblages. Chlorite associated with late alteration at Sossego (−63‰) and epidote from Sequeirinho ore (−6‰) and late veins in gabbro (−10 to −5‰) were also analyzed (Table 6).

The hydrogen isotope fractionation factors of Graham et al. (1984) for actinolite–water, and Graham et al. (1987) for chlorite–water were used to calculate δD_{H2O} values. For the epidote–water fractionation, the equations of Graham et al. (1980) and Chacko et al. (1999) give conflicting results that differ by 12‰ at 200°C. For this study, we have followed the recommendation of Morrison (2004) to adopt the equation of Chacko et al. (1999).

The calculated δD_{H2O} values for fluids in equilibrium with regional actinolite are −47±5‰ at 500±25°C. At Sequeirinho, actinolite from Na–Ca alteration (−41±5‰ at 500±25°C), actinolitite (−42±7‰ at 550±25°C) and mineralized breccia (−42±5‰ at 400±50°C) indicate a narrow range of δD_{H2O} values. For the Sossego orebody, calculated δDH_2O values from actinolite vary from −41 to −62‰ at 400±50°C. The δD_{H2O} values for ore-related epidote from Sequeirinho (19±5‰; 230±25°C), and for late mineralized gabbro-hosted veins at Baiano (10 to 15‰; 200±25°C) are unreasonably high (Fig. 11). As epidote is highly susceptible to retrograde equilibration, and its use in inferring δD_{H2O} values has been the subject of controversy (Kyser and Kerrich 1991; Dilles et al. 1992), δD_{H2O} values from epidote must be considered with caution. Postmineralization chlorite from Sossego yields an intermediate δD_{H2O} of −35‰ (250±25°C) (Fig. 11).

Carbon isotopes

Carbon isotope analyses were carried out on calcite from mineralized veins and breccias from the Sossego–Curral orebodies (Table 5). Calcite from mineralized breccias at Sequeirinho and veins that crosscut magnetite ± albite ± actinolite replaced gabbro from the Sequeirinho–Baiano orebodies was also analyzed. Narrow carbon isotopic variation was found for calcite from the Sossego deposit ($\delta^{13}C$=−6.1±2.3‰; n=36). Assuming that carbon was speciated as H_2CO_3 during ore formation and that H_2CO_3 isotopically behaves like CO_2, the isotopic fractionation factor for carbon between calcite and CO_2 of Ohmoto and Rye (1979) was used to calculate the carbon isotopic composition of the fluid. Calculated $\delta^{13}C_{H^2CO^3}$ values for Sequeirinho calcite (−4.7±1.4‰, at 230±25°C) and Sossego calcite I (−4.0±1.2‰, at 400±50°C), calcite II (−3.8±0.6‰, at 275±25°C), and calcite III (−3.4±0.9‰, at 250±25°C) are similar. For calcite veins in hydrothermalized gabbro from

Table 6 Hydrogen isotope composition of hydrous silicates from the Sossego IOCG deposit

Sample	Mineral	δD_{min} (‰)	T (°C)[a]	δD_{fluid} (‰)[b]
Sequeirinho				
Regional Na–Ca alteration				
Sos 10A	Actinolite	−76	500±25	−47±5
Na–Ca alteration				
280/488,67	Actinolite	−70	500±25	−41±5
Actinolitite				
Sos 39K	Actinolite	−69	550±25	−40±5
Sos 39L	Actinolite	−68	550±25	−39±5
99/296,07	Actinolite	−71/−70	550±25	−42±5
259/264,60	Actinolite	−74	550±25	−45±5
352/122,80	Actinolite	−70	550±25	−41±5
Breccia infilling				
22/312,67	Actinolite	−71	400±50	−42±5
38C	Epidote	−6	230±25	19±5
Baiano (vein in gabbro)				
279/126,68	Epidote	−10	200±25	10±5
279/154,08	Epidote	−5	200±25	15±5
Sossego (vein/breccia infilling)				
319/113,92	Chlorite	−63	250±25	−35±5
319/113,92	Actinolite	−70	400±50	−41±5
319/150,29	Actinolite	−72	400±50	−43±5
319/152,92	Actinolite	−70	400±50	−41±5
419/136,94	Actinolite	−93/−88	400±50	−62±5

[a] Temperature intervals represent calculated oxygen isotope temperatures for mineral pairs and conditions estimated from geothermobarometry and mineral stability fields. See text for discussions.

[b] Mineral–water fractionations calculated from Chacko et al. (1999) and Graham et al. (1984, 1987).

the Sequeirinho–Baiano oredodies, wider isotopic variation is observed (−5.0±3.2‰, at 240±50°C).

On a $\delta^{13}C$ vs $\delta^{18}O$ plot (Fig. 12a), a significant isotopic covariation of carbon and oxygen may be observed only for the calcite from veins in gabbro.

A comparison of carbonate data from Sossego and other IOCG deposits in the CMP (Fig. 12b) indicates that, except for gabbro-hosted veins at Sequeirinho–Baiano, $\delta^{18}O$ and $\delta^{13}C$ values have narrow ranges. Similarly, narrow ranges are also found in the Gameleira deposit

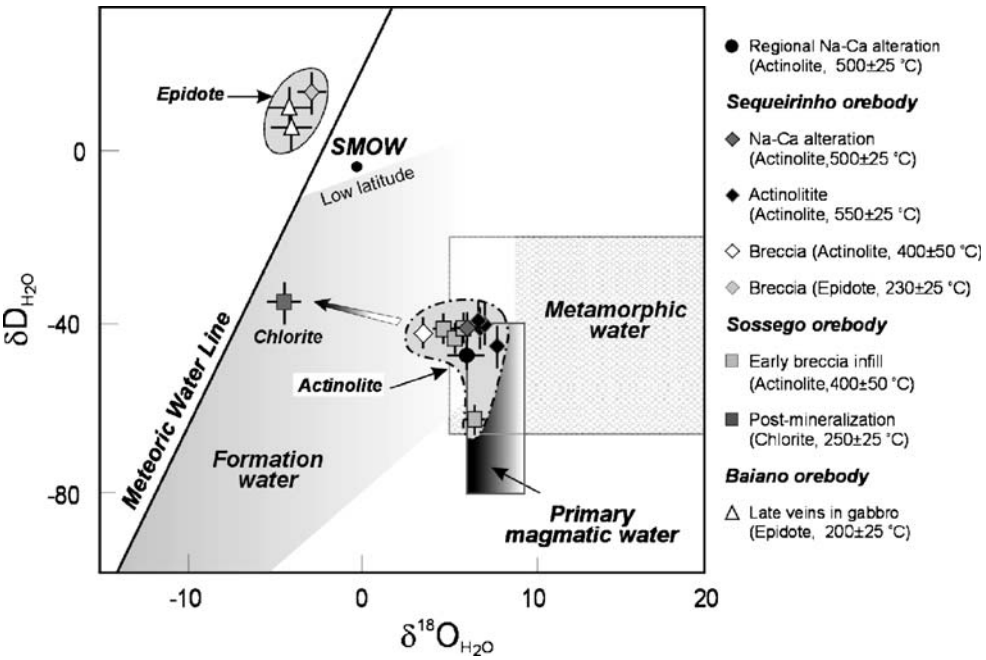

Fig. 11 Calculated oxygen and hydrogen isotope compositions for the fluids associated with the hydrothermal alteration and mineralization of the Sossego IOCG deposit. Hydrogen isotope fractionations: epidote–H_2O (Chacko et al. 1999); actinolite–H_2O (Graham et al. 1984); chlorite–H_2O (Graham et al. 1987). Oxygen isotope fractionations: actinolite–H_2O; epidote–H_2O; chlorite–H_2O (Zheng 1993b)

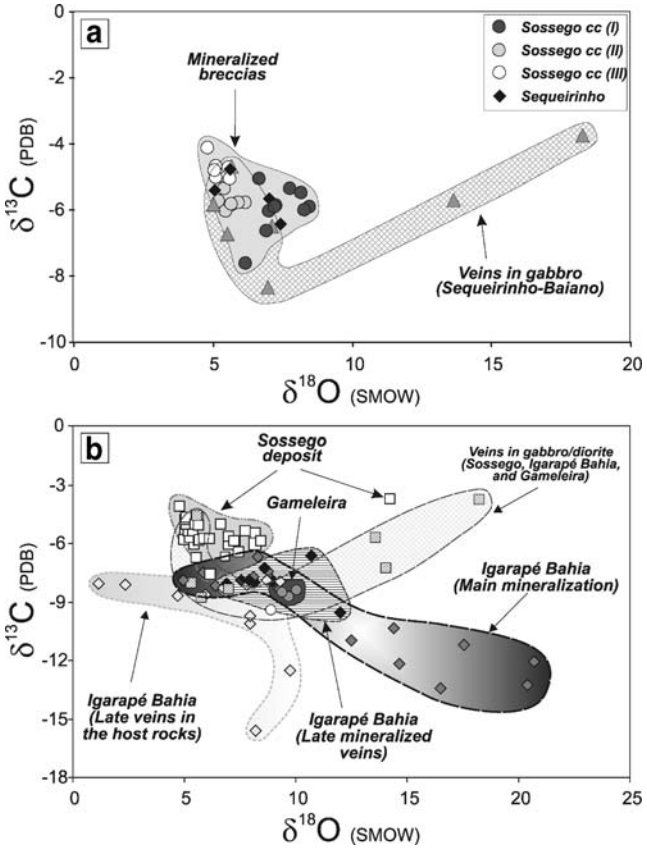

Fig. 12 **a** Oxygen and carbon isotopic data for carbonates from the Sossego IOCG deposit. Data from Monteiro et al. (submitted) and this study; **b** oxygen and carbon isotopic data for carbonates from the Carajás IOCG deposits. Data from Igarapé Bahia: Dreher (2004); Gameleira: Lindenmayer et al. (2002)

(Lindenmayer et al. 2002) and late veins from Igarapé Bahia (Dreher 2004). However, in the latter deposit, carbonate from the main mineralization stage shows wide isotopic variation and a negative correlation between $\delta^{13}C$ and $\delta^{18}O$ (Dreher 2004). Additionally, carbon and oxygen compositions of calcite from veins that crosscut gabbro in other deposits (e.g., Igarapé Bahia and Gameleira) are within the same covariant trend identified at the Sossego deposit (Fig. 12b).

Sulfur isotopes in sulfides

Sulfur isotope compositions of chalcopyrite were determined for the Sossego–Curral (5.7±1.9‰; n=25), Sequeirinho (4.6±1.6‰; n=15), Baiano (5.6±0.5‰; n=2), and Pista (2.5±0.3‰; n=5) orebodies (Table 7; Figs. 13 and 14). Additional analyses of a Sequeirinho pyrite gave a $\delta^{34}S$ value of 3.5‰, and of Pista molybdenite gave a value of 2.4‰. The lowest $\delta^{34}S$ values are from sulfide veins along mylonitic foliations in metavolcanic rocks of the Pista orebody, whereas the highest $\delta^{34}S$ values (>6‰) are displayed by veins and breccias from the other orebodies.

At Sequeirinho, chalcopyrite ($\delta^{34}S$=4.2‰) in heavier than adjacent pyrite ($\delta^{34}S$=3.5‰). This is the reverse of the fractionation expected if the two minerals were deposited in equilibrium, but is consistent with petrographic studies that indicate chalcopyrite deposition postdated pyrite formation.

Discussion

Temporal and vertical zonation in the Sossego system

The Sossego deposit contains hydrothermal alteration zones similar to those recognized at other IOCG deposits. The Pista–Sequeirinho–Baiano orebodies display a generally consistent pattern of early regional sodic alteration (albite–hematite) followed by sodic–calcic alteration (actinolite–albite), which was associated with the formation of magnetite–(apatite) replacement bodies. Sodic and sodic–calcic alteration types in most IOCG districts are typically developed below or peripheral to potassic alteration assemblages (Hitzman et al. 1992). The magnetite–(apatite) replacement bodies at Pista–Sequeirinho–Baiano are similar, in terms of style of mineralization and associated alteration, to magnetite bodies developed in a number of localities worldwide which are generally termed "Kiruna-type" deposits (Hitzman 2000). Sodic–calcic alteration in the Sossego deposit was followed by weakly developed potassic alteration and then a complex, epidote-dominant calcic alteration stage that marked the beginning of significant sulfide precipitation.

The Sossego–Curral orebodies are characterized by well−developed potassic alteration that grades laterally outward to a zone of chloritization (Fig. 15). This potassic assemblage is cut by a later assemblage of calcite–chlorite–epidote–muscovite–sulfides and a late sericite–hematite–quartz–chlorite–calcite (hydrolytic) assemblage. These lower temperature alteration assemblages are interpreted to represent a structurally higher level than the sodic and sodic–calcic assemblages at Sequeirinho. Thus, the E–W-trending fault that separates the Pista–Sequeirinho–Baiano orebodies from the Sossego–Curral orebodies is believed to have significant vertical displacement. However, the absence of well-defined marker horizons within the stratigraphy makes determination of the exact amount of offset impossible to determine.

Sulfide mineralization began during the potassic alteration event, but intensified after potassic alteration. Mineralized breccias contain an early assemblage represented by coarse-grained zoned actinolite/ferroactinolite, Cl–apatite, and magnetite. Sulfide mineralization was associated with paragenetically late epidote–chlorite–allanite–calcite–quartz–titanite assemblage. In the Pista–Sequeirinho–

Table 7 Sulfur isotope analyses in sulfides from the Sequeirinho and Sossego orebodies of the Sossego IOCG deposit

Sample	Mineral		$\delta^{34}S$ (‰ CDT)
Pista orebody			
SOS 346/85.00	Molybdenite	Chalcopyrite–molybdenite veinlet	2.4
SOS 346/93.0	Chalcopyrite	Chalcopyrite vein along the mylonitic foliation	2.3
SOS 346/85.00	Chalcopyrite	Chalcopyrite–molybdenite veinlet	2.8
SOS 346/161.0	Chalcopyrite	Calcite–chlorite–biotite–quartz–chalcopyrite vein	2.2
SOS 346/185.00	Chalcopyrite	Chalcopyrite–quartz–calcite–epidote vein	2.3
Sequeirinho orebody			
SOS 99/304.23	Pyrite	Chalcopyrite–pyrite–magnetite in ore breccia	3.5
SOS 99/304.23	Chalcopyrite	Chalcopyrite–pyrite–magnetite in ore breccia	4.2
SOS 280/421.4	Chalcopyrite	Chalcopyrite–albite–epidote–actinolite veinlets in altered gabbro	3.8
SOS 280/423.0	Chalcopyrite	Chalcopyrite–albite–epidote–actinolite veinlets in altered gabbro	3.7
SOS 352/196.7	Chalcopyrite	Chalcopyrite veins in Na–Ca altered rock	4.0
SOS 352/204.0	Chalcopyrite	Chalcopyrite veins in Na–Ca altered rock	3.4
SOS 22/273.78	Chalcopyrite	Chalcopyrite veinlets in actinolitite/magnetitite	3.1
SOS 99/332.28	Chalcopyrite	Chalcopyrite–pyrite–magnetite in ore breccia	2.9
SOS 259/263.87	Chalcopyrite	Chalcopyrite–pyrite–magnetite–apatite in ore breccia	4.1
SOS 259/268.00	Chalcopyrite	Chalcopyrite–pyrite–magnetite–apatite in ore breccia	3.0
SOS 259/270.25	Chalcopyrite	Chalcopyrite–pyrite–magnetite–apatite in ore breccia	3.2
SOS 259/273.7	Chalcopyrite	Chalcopyrite–actinolite–apatite in the ore breccia	3.2
SOS 39D	Chalcopyrite	Massive chalcopyrite (ore breccia matrix)	6.3
SOS 39K	Chalcopyrite	Massive chalcopyrite (ore breccia matrix)	6.0
SOS 39L	Chalcopyrite	Massive chalcopyrite (ore breccia matrix)	4.2
Baiano orebody			
SOS 279/283.28	Chalcopyrite	Calcite–chlorite–chalcopyrite vein in altered gabbro	6.1
SOS 279/283.65	Chalcopyrite	Calcite–chalcopyrite vein in altered gabbro	5.1
Sossego/Curral orebodies			
SOS 319/154.9	Chalcopyrite	Calcite II–actinolite–apatite–magnetite–chalcopyrite vein	4.5
SOS 419/56.73	Chalcopyrite	Calcite II–actinolite–apatite–magnetite–chalcopyrite vein	3.8
SOS 419/101.59	Chalcopyrite	Calcite II–actinolite–apatite–magnetite–chalcopyrite (breccia matrix)	4.0
SOS 419/136.94	Chalcopyrite	Calcite II–actinolite–apatite-chalcopyrite (ore breccia matrix)	5.8
SOS 314/200.0	Chalcopyrite	Calcite II–actinolite–apatite–chlorite–chalcopyrite (breccia matrix)	4.0
SOS 314/255.3	Chalcopyrite	Calcite II–actinolite–apatite–chlorite–chalcopyrite (breccia matrix)	4.3
SOS 314/299.0	Chalcopyrite	Calcite II–actinolite–apatite–chlorite–chalcopyrite (breccia matrix)	4.4
SOS 314/166.8	Chalcopyrite	Calcite II–quartz–apatite–chlorite–chalcopyrite (breccia)	4.2
SOS 314/195.90	Chalcopyrite	Calcite II–quartz–apatite–biotite–chlorite–chalcopyrite (breccia)	5.6
SOS 314/198.05e	Chalcopyrite	Calcite II–quartz–apatite–chlorite–chalcopyrite (breccia matrix)	5.7
SOS 314/198.05f	Chalcopyrite	Calcite II–quartz–apatite–chlorite–chalcopyrite (breccia matrix)	7.0
SOS 419/147.00	Chalcopyrite	Calcite II–quartz–apatite–chalcopyrite (ore breccia matrix)	5.0
SOS 314/132.90	Chalcopyrite	Calcite II–quartz–chalcopyrite (breccia matrix)	5.8
SOS 314/149.45	Chalcopyrite	Calcite II–quartz–chalcopyrite (breccia matrix)	5.3
SOS 319/150.29	Chalcopyrite	Calcite–chalcopyrite–actinolite–quartz–chlorite (breccia matrix)	6.1
SOS 319/152.92	Chalcopyrite	Calcite III–chlorite–actinolite–apatite–chalcopyrite vein	7.6
SOS 319/112.02	Chalcopyrite	Calcite III–actinolite-chlorite–chalcopyrite vein	6.2
SOS 319/172.46	Chalcopyrite	Calcite III–quartz–chlorite–chalcopyrite (breccia matrix)	6.9
SOS 319/57.77	Chalcopyrite	Massive chalcopyrite (ore breccia)	6.1
SOS 319/79.70	Chalcopyrite	Massive chalcopyrite (ore breccia)	4.9
SOS 35/159.20	Chalcopyrite	Calcite–actinolite–apatite–chalcopyrite (vein)	4.8
SOS 35/86.23	Chalcopyrite	Calcite–actinolite–apatite–chalcopyrite (vein)	4.1
SOS 35/506.88	Chalcopyrite	Calcite–actinolite–apatite–chalcopyrite (breccia matrix)	6.7
SOS 35/696.80	Chalcopyrite	Calcite–quartz–chlorite–chalcopyrite (breccia matrix)	6.4
SOS 35/720.75	Chalcopyrite	Calcite–quartz–chlorite–chalcopyrite (breccia matrix)	6.6

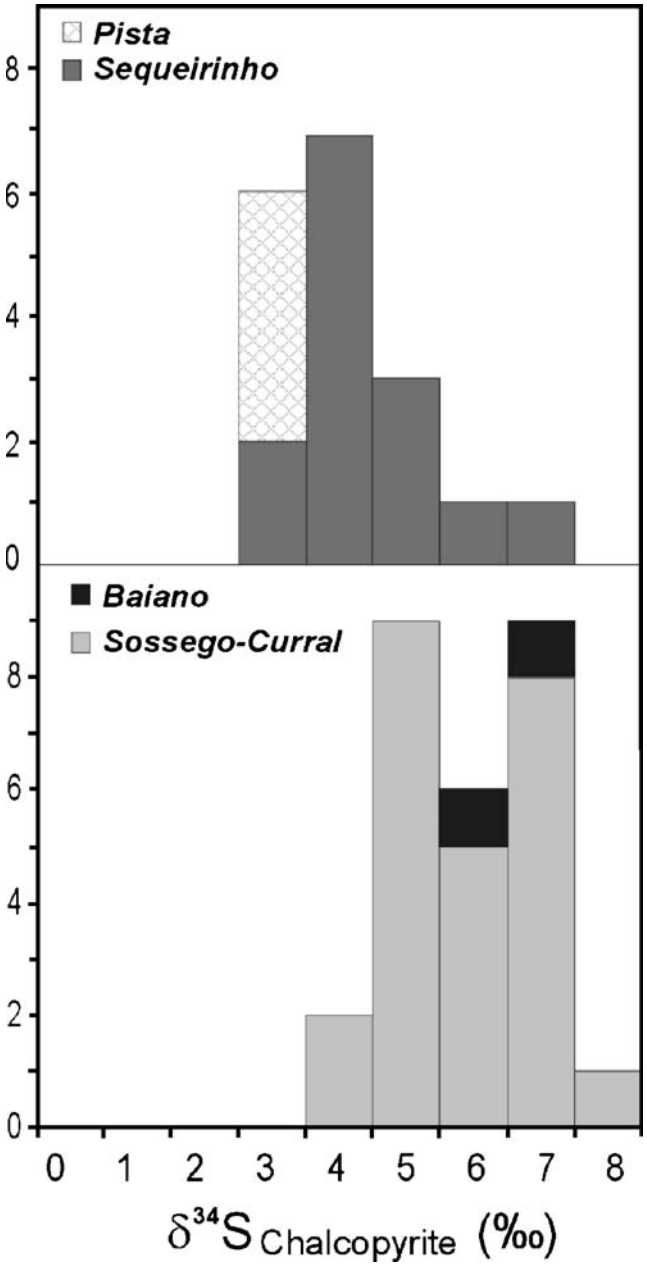

Fig. 13 Distribution of the $\delta^{34}S$ values of sulfides at the Sequeirinho, Pista, Baiano, Curral and Sossego orebodies in the Sossego IOCG deposit

Baiano orebodies, the sodic and sodic–calcic alteration assemblages commonly display ductile fabrics and sulfides are locally deformed. In contrast, calcite–quartz and sulfides in the Sossego/Curral orebodies fill open space indicating brecciation and mineral precipitation in a brittle structural environment. The sulfide assemblage at Sequeirinho is dominated by chalcopyrite but locally contains significant pyrrhotite and pyrite. At Sossego–Curral the sulfide assemblage is dominated by chalcopyrite and pyrite but lacks pyrrhotite.

The structurally highest and latest alteration assemblage at Sossego–Curral is a hydrolytic assemblage of sericite–hematite–calcite–quartz–chlorite, which is also present at Pista. This relatively barren assemblage could mark an influx of meteoric water into the system, based on $\delta^{18}O$ fluid compositions, with an increase in oxygen fugacity and a decrease in pH.

The complex stages of sodic, sodic–calcic, potassic, and hydrolytic alteration observed at Sossego are generally similar to those described by Marschik and Fontboté (2001) from the Candelaria–Punta del Cobre IOCG system in Chile. The temporal and vertical zonation observed in the Sossego system generally fits the "classical" system of alteration zoning predicted in IOCG systems (Hitzman et al. 1992; Haynes 2000). Approximately 450 m of vertical section is present in both the Sequeirinho and Sossego–Curral orebodies. The amount of displacement along the fault separating the orebodies is not easily calculated, but may be several hundred meters. Thus, it appears that the Sossego deposit provides a vertical view of at least 1.5 km though a major IOCG hydrothermal system.

The Sossego deposit also appears to record hydrothermal alteration during the transition from a dominantly brittle–ductile to a dominantly brittle structural regime. This could be, at least partially, related to episodic decompression due to fluid overpressuring and hydrofracturing. Early sodic alteration was pervasive, due to infiltration of hydrothermal fluids along a myriad of fine fractures and along grain boundaries. This pervasive albitization cut and was cut by shear zones with brittle–ductile, mylonitic fabrics. Later, sodic–calcic alteration was also controlled by the shear zone development. Fluid flow related to these early alteration stages was controlled by permeability in large-scale regional shear zones enhanced by interconnected fault planes. Potassic alteration assemblages were fracture-controlled, though pervasive alteration zones are locally present. Late sulfide mineralization reflects essentially brittle conditions in both Sequeirinho and Sossego segments. However, while ductile-deformed sulfides are locally present at Sequeirinho, they are absent at Sossego–Curral. Well-developed vuggy breccias with open space filling textures are present only at Sossego–Curral.

Fluid sources and evolution of the hydrothermal system

Evolution of the hydrothermal system was accompanied by sharp temperature decline and decrease of $\delta^{18}O_{H_2O}$ values through the paragenesis (Fig. 10) in the different orebodies. At Sequeirinho, massive magnetite and actinolitite were formed by high temperature (550±25°C), high $\delta^{18}O_{H_2O}$ fluids (6.9±0.9‰). Sodic–calcic and sodic alteration (Fig. 15) developed in the presence of fluids with $\delta^{18}O_{H_2O}$ values of 6.0±0.8‰ (500±25°C), and 3.6±0.6‰ (450±50°C), respectively.

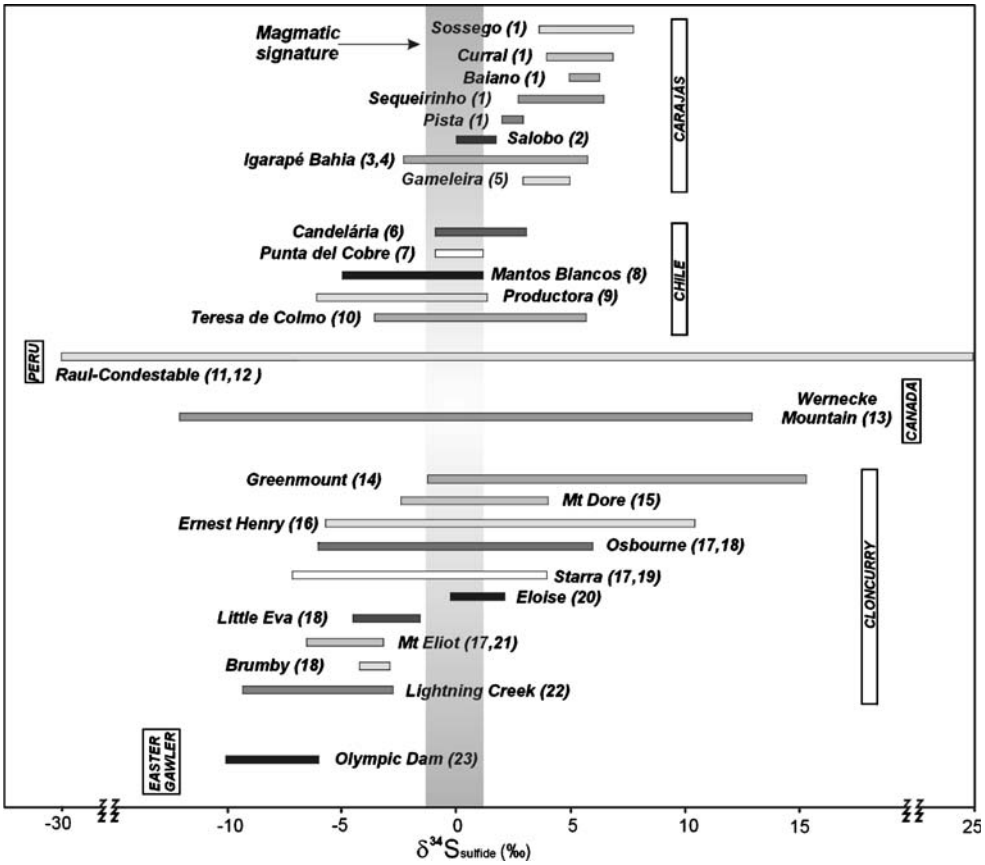

Fig. 14 Sulfur isotopic compositions of sulfides from the Sossego IOCG deposit and other IOCG deposits in the CMP and worldwide. Sources of data: (1) this study; (2) Réquia and Fontboté (2001); (3) Tavaza and Oliveira (2000); (4) Dreher (2004); (5) Lindenmayer et al. (2002); (6) Marschik and Fontboté (2001); (7) Marschik et al. 2000 (8) Ramírez et al. (2006); (9) Fox and Hitzman (2001); (10) Ledlie (1988); (11) Ripley and Ohmoto (1977); (12) Haller et al. (2002); (13) Hunt et al. (2005); (14) Krcmarov (1995); (15) Beardsmore (1992); (16) Twyerould (1997); (17) Davidson and Dixon (1992); (19) Pollard et al. (1997); (20) Rotherham et al. (1998); (21) Baker et al. (2001); (22) Garrett (1992); (23) Perring et al. (2001); (24) Eldridge and Danti (1994)

The δD_{H2O} and $\delta^{18}O_{H_2O}$ values of fluids that formed Na–Ca alteration and actinolitite partially overlap the characteristic range for primary magmatic waters and low-temperature metamorphic waters (Taylor 1997; Fig. 11). These same $\delta^{18}O_{H_2O}$ values could also have resulted from high temperature equilibration of deeply circulating basinal or formational/meteoric waters with the host rock units. Outwards from the magnetite bodies in the deep parts of the system (Fig. 15), early regional sodic alteration assemblages require fluids with $\delta^{18}O_{H_2O}$ values (3.8±0.3‰) below those typical of magmatic fluids. This may imply that the large volumes of sodic alteration were formed by ^{18}O-depleted externally derived fluids. The distribution of the sodic alteration zone suggests that this fluid was progressively more important upwards in the system and later in the hydrothermal paragenesis.

The copper–gold mineralization at Sossego was formed by the lower $\delta^{18}O_{H_2O}$ fluid. In the deeper Sequeirinho orebody, this stage was marked by a sharp decline in temperature to below 250°C, and by the presence of ^{18}O-depleted (−1.8±3.4‰) hydrothermal fluids. In the Sossego–Curral orebody, temperatures decreased from >450°C in the potassic and late sodic–calcic alteration stages to >300°C in the mineralization stage. As temperature decreased, $\delta^{18}O_{H_2O}$ evolved from 8.4±1.6‰ in the early vein and breccia infilling to 1.5±2.1‰ in the mineralization stage and −3.3±3.2‰ in the hydrolytic alteration stage. The relatively high δD_{H2O} value (−35‰) implied by chlorite suggests that δD_{H2O} increased in the late alteration stage.

The decrease of $\delta^{18}O_{H_2O}$ values through the paragenesis (Fig. 10) may reflect, at least partially, retrograde exchange between early minerals and the ^{18}O-depleted mineralizing fluids. This is suggested especially for early actinolite and apatite within the breccia matrix at Sequeirinho because these minerals commonly are altered along grain boundaries and fractures. Wider isotopic variation shown by apatite could be explained by this process. However, oxygen isotope compositions of syn–ore minerals, mainly quartz, possibly reflect the signature of the mineralizing fluid because postmineralization alteration (e.g., hydrolytic alteration) was restricted, notably at Sequeirinho.

Participation of externally-derived ^{18}O-depleted and relatively D-enriched fluids likely reflects the influx of another fluid during the mineralization stage. $\delta^{18}O_{H_2O}$ and δD_{H2O} values down to nearly −6.5 and −35‰, respectively, recorded by late chlorite, are not consistent with seawater, but point to a predominantly meteoric origin.

Surficial water contribution was invoked for the Olympic Dam IOCG deposit (Oreskes and Einaudi 1992), where

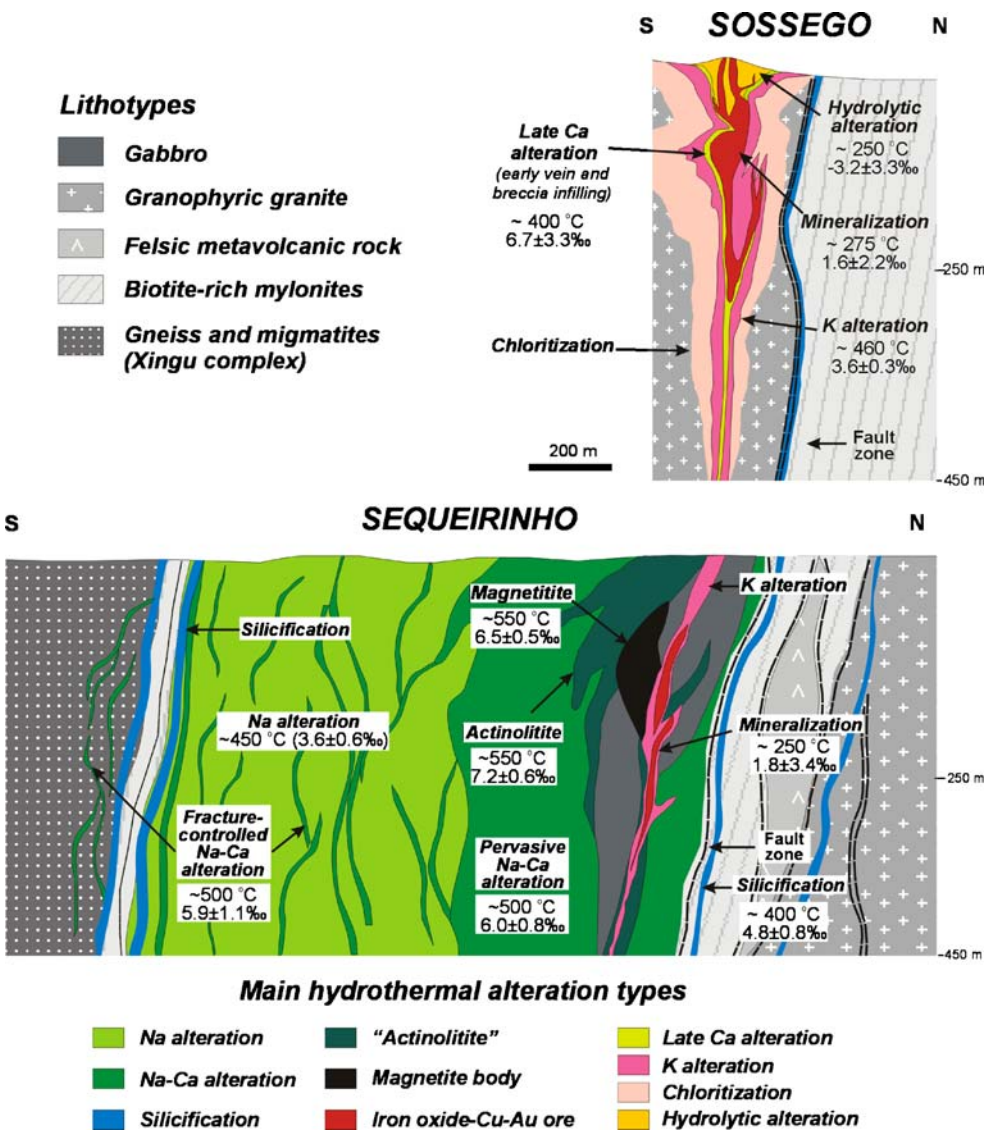

Fig. 15 Schematic profile of the Sequeirinho and Sossego orebodies showing distribution of hydrothermal alteration zones and average temperature and oxygen isotope composition of the hydrothermal fluids involved in each alteration stage

ore deposition was related to mixing of a cool surficial fluid that had variable salinity and low $\delta^{18}O_{H_2O}$ values ranging from −2 to +6‰ and warmer, more saline, deep-seated fluid (Oreskes and Einaudi 1992). At Candelária and Punta del Cobre, Chile (Marschik and Fontboté 2001), and in the Cloncurry district, Australia (Mark et al. 2004) surficial fluids possibly contributed only to postmineralization late stages of hydrothermal activity. In Cloncurry, participation of basinal brine or low latitude, low-elevation meteoric water in postmineralization hydrothermal events was inferred from epidote δD values (Mark et al. 2004).

In the Sossego deposit, Na, Na–Ca, and later potassic alteration, and sulfide mineralization possibly comprise part of a geochemically coupled hydrothermal system. Stable isotope data suggest interplay of two different fluids in the system: (1) high temperature (>500°C), ^{18}O-enriched, deep-seated fluid, which may represent formational/metamorphic waters possibly involving magmatic components, and (2) low to moderate temperature (<300°C), ^{18}O-depleted meteoric–hydrothermal fluids. Extent of mixing of these fluids may have been controlled by fluctuations in space and time of pore pressure and permeability.

Fluid inclusion studies carried out on quartz from mineralized veins and breccias from the Sossego orebody (Carvalho et al. 2005) revealed the coexistence of two aqueous fluids: (1) halite-bearing (S-L-V) aqueous inclusions with high salinities (32–69 wt% NaCl equiv) and temperatures (200–570°C); and (2) two-phase (L-V) fluid inclusions with lower homogenization temperatures (102 to 312°C) and variable salinities (2–23.6 wt% NaCl equiv). These fluids could correspond to deep-seated and meteoric–hydrothermal fluids, respectively. The salinity vs total homogenization temperature relationship indicates that the initially high-temperature (>500°C) and high-salinity (~70 wt%) fluid was progressively diluted with temperature decrease. The two-phase fluid presents a tenden cy of increasing salinity accompanied by temperature

decrease. Relatively high-temperature (~300°C) fluids have the lowest salinities, reflecting the channeled nature of meteoric fluids, which may episodically be related with overpressure, whereas the salinity increase and temperature decrease may be explained by interaction of this hot meteoric fluid with the host rocks at low fluid/rock ratios (Monteiro et al., submitted).

The narrow range of oxygen and carbon isotopic values of hydrothermal carbonates from veins and breccias of the Sossego/Curral and Sequeirinho orebodies are not typical of extensive fluid mixing. However, as carbonate is usually sensitive to alteration, homogenization of the oxygen isotopic compositions of the early carbonate phase (calcite I), at high water/rock ratios, cannot be ruled out. This could have obliterated original oxygen and carbon isotopic covariations due to overprinting of the alteration process. Precipitation of calcite II associated with equant quartz crystals in the main mineralization stage at Sossego occurred at near equilibrium conditions, possibly due to decrease of salinity of the hydrothermal fluids. Thus, calcite and quartz precipitation could result from dilution associated with input of the meteoric fluids in the system.

Additionally, carbon and oxygen isotopic covariation observed in calcite from late gabbro-hosted veins in the Sequeirinho–Baiano orebodies, could be explained by fluid-rock interaction along open rock fractures involving relatively hot meteoric–hydrothermal fluids (~300°C) and cold ^{18}O-enriched host gabbro at relatively low W/R ratios.

Precipitation of hydrothermal minerals in early hydrothermal stages may have contributed to fault sealing and permeability decrease, preventing extensive and progressive fluid mixing. Therefore, transition from a dominantly brittle–ductile to a dominantly brittle structural regime that marks the mineralization stage in the Sossego ore system could be, at least partially, related to episodic decompression due to fluid overpressuring. These episodic events might have permitted influx of channeled meteoric water in the system that caused dilution and cooling of an initially high-temperature (>500°C) high-salinity deep-seated fluid. This could explain the sharp decrease of temperature and $\delta^{18}O_{H_2O}$ values related to different infilling stages of veins and breccias. This process would be also responsible for deposition of metals transported as metal chloride complexes, causing the bulk ore precipitation.

Carbon and sulfur sources

Calculated $\delta^{13}C_{CO^2}$ values for the Sossego–Curral and Sequeirinho mineralized breccias are −4.3±1.8‰. The values are similar to those of magmatic carbon, pristine mantle, and volcanic CO_2, which have $\delta^{13}C$ ~−5‰; Ohmoto (1986). However, the average $\delta^{13}C$ value of the crust is also about −5‰; a value that can be generated through so many different pathways that it is not diagnostic of a mantle origin (Ohmoto and Goldhaber 1997). The carbon signature at Sossego possibly reflects $\delta^{13}C_{CO^2}$ values similar to those of the surrounding rocks.

In the Sossego system, all orebodies show heavier sulfur ($\delta^{34}S$=4.9±2.4‰) than expected for a mantle source ($\delta^{34}S$=0±1‰; Eldridge et al. 1991). Sulfide $\delta^{34}S$ values increase from 2.2‰ at Pista to up to 7.6‰ at Sossego-Curral.

For the Pista orebody, the occurrence of pyrrhotite as a stable sulfide mineral may suggest that the mineralizing fluid was in the H_2S predominant field. Hence, the sulfide $\delta^{34}S$ values would be expected to closely reflect $\delta^{34}S_{\sum s}$. This could be also valid for the other orebodies; however, the occurrence of magnetite as a stable mineral may imply the coexistence of oxidized and reduced sulfur species in the fluid. Therefore, the $z\delta^{34}S_{\sum s}$ values could have been significantly higher than the $\delta^{34}S$ values of sulfide mineral phases, suggesting a relatively heavy sulfur source for breccia sulfides. This needs to be confirmed by evaluation of the sulfate sulfur isotopic composition of other phases, such as epidote, apatite, and barite, which were found as inclusions in potassium feldspar. However, fractionation at high oxidation state commonly results in a wide isotopic range (Davidson and Dixon 1992), which was not identified in the Sossego system.

Despite uncertainties regarding total sulfur composition in the system, possible sulfur sources in the range of 2 to 8‰ would be:

(1) Inorganically reduced Archean seawater sulfate/evaporite with $\delta^{34}S$ values of ~2 to 5‰ during the interval of ~3.5 to ~2.7 Ga and a gradual increase to 10‰ at ~2.5 Ga (Strauss 1993; Ohmoto and Goldhaber 1997);
(2) Inorganically reduced sulfate from continental evaporites (~10‰);
(3) Leached magmatic rocks or fluids from magmas that acquired most of their sulfur by assimilation of country rocks.

According to Ohmoto and Goldhaber (1997), it has become apparent that igneous rocks with $\delta^{34}S$ values different from 0±5‰ are quite common, vary regionally, and have sulfur isotopic compositions similar to those in country rocks. A considerable proportion of sulfur in the igneous rocks may have been obtained from the country rocks by bulk or selective assimilation. Sulfur sources for magmatic–hydrothermal systems, notably those that formed porphyry and skarn deposits (Ohmoto and Goldhaber 1997), have been shown to include assimilated country rock sulfur. Examples include the porphyry-type Cu–Mo mineralization at Butte, Montana, where total sulfur was

isotopically heavy (10‰), and would have required an evaporitic crustal component to the relatively oxidized granitic parental magma that was the source of the hydrothermal fluids and sulfur (Field et al. 2005).

In the Sossego system, the three potential sulfur sources outlined above cannot be distinguished using the present data. Oxidized, meteoric fluid may have introduced ^{34}S-enriched (up to 7.6‰) SO_4^{2-} from surficial reservoirs, including continental evaporites, into the system late in the paragenesis, although complete reduction to H_2S is suggested by the narrow $\delta^{34}S$ range in the orebodies themselves. Alternatively, sulfur derivation from leaching of host rocks, including metavolcano–sedimentary with metaevaporitic layers and igneous rocks could be suggested. This would imply a long-lived fluid-rock interaction process involving hot deep-seated fluids.

Sulfur isotope ratios of sulfides (Fig. 14) from IOCG deposits worldwide span a wide range (−31 to +26‰, Fig. 14), although individual deposits may exhibit mode and mean values close to 0‰, including Osborne, Starra, Ernest Henry, and Eloise in the Cloncurry Province, Australia (Davidson and Dixon 1992; Williams and Pollard 2003) and Candelária, Punta del Cobre, Productora, Mantos Blancos, Teresa del Como, in Chile (Marschik and Fontboté 2001; Fox and Hitzman 2001; Ramírez et al. 2006). The near-zero signatures have been considered as compatible with a predominantly magmatic source (i.e., sulfur from a magmatic fluid phase or leached from igneous rocks; Baker et al. 2001; Marschik and Leveille 2001; Twyerould 1997; Rotherham et al. 1998; Williams and Pollard 2003), although coupled variations in temperature, pH, oxygen fugacity, and mixing with metasedimentary sulfur would be necessary to explain the observed deposit-to-deposit variations (Williams and Pollard 2003).

Light sulfur signatures ($\delta^{34}S<-3$‰) are found in sulfides from the Cloncurry (e.g., Mt Elliot, Little Eva, Brumby, Lightning Creek) and Easter Gawler (e.g., Olympic Dam) districts. These signatures probably reflect the relatively high oxidation state of the ore stage. Under oxidizing conditions there is a large negative isotopic fractionation between sulfides and aqueous sulfur, which in Cloncurry and Easter Gawler is thought to have been magmatic in origin (Davidson and Dixon 1992).

However, the sulfur isotopic variations that have been observed in IOCG deposits could also imply other sulfur sources besides the magma. According to Barton and Johnson (1996), in a number of IOCG deposits worldwide isotopically heavy sulfur ($\delta^{34}S>5$‰) may implicate non-magmatic sulfur sources. For the Starra and Osborne deposits, Cloncurry district, possible sulfur sources include magmatic sulfur, and also inorganically reduced seawater sulfate, continental evaporite sulfur, or leached sedimentary sulfur (Davidson and Dixon 1992).

Extreme $\delta^{34}S$ variations in the IOCG deposits at Raúl-Condestable, Peru (−31.1 to 26.3‰; Ripley and Ohmoto 1977; Haller et al. 2002), and Wernecke Mountain, Yukon, Canada (−12 to 13‰; Hunt et al. 2005) might also indicate a strong sulfur contribution of marine/evaporite sulfate and biogenic sulfur contained in sediments (Ripley and Ohmoto 1977; Haller et al. 2002).

Thus, sulfide $\delta^{34}S$ may reflect variation in physical–chemical conditions (fO_2, T, pH) during ore deposition, different sulfur isotopic signatures in country rocks, or multiple sulfur sources for individual systems.

Carajás IOCG deposits

The Sossego deposit shares common characteristics with other IOCG deposits of the CMP including: (1) the nature of the host rocks (all deposits are included in units of the Itacaiúnas Supergroup); (2) spatial relation to shear zones and to intrusions of different compositions; (3) intense hydrothermal alteration with a progression from early sodic alteration to later potassic alteration and finally sulfide mineralization; and (4) variable fluid inclusion homogenization temperatures (100–570°C) and salinities (0 to 69 wt% NaCl eq.) in ore-related minerals (Table 1).

Genetic models for these deposits have emphasized the importance of Late Archean (~2.57 Ga) and/or Paleoproterozoic (~1.88 Ga) granite intrusions for the evolution of magmatic-hydrothermal systems (e.g., Tallarico et al. 2005; Tavaza and Oliveira 2000; Réquia et al. 2003; Pimentel et al. 2003). However, dating of ore-related minerals has revealed different ages in a single deposit (e.g., Igarapé Bahia, Gameleira, Salobo; Réquia et al. 2003; Tallarico et al. 2005; Pimentel et al. 2003). These ages may not be clearly related to an individual magmatic event implying a prolonged hydrothermal history. Thus, despite the importance of Archean and Paleoproterozoic magmatism in the CMP, which could provide heat for the establishment of extensive hydrothermal systems, the long-term evolution of these systems is still to be unraveled.

Recent studies on the IOCG deposits in the CMP point to the importance of alternative sources to magma-derived brines to explain the ubiquitous presence of highly saline fluids in the Fe oxide–Cu–Au deposits from the CMP. Boron isotope studies indicate high $\delta^{11}B$ values (12.6 to 26.6‰) for the ore-related Igarapé Bahia tourmaline that could represent indirect evidence of a marine evaporitic contribution to the hydrothermal system (Xavier et al. 2005). Highly saline fluids could also derive from a burial metamorphism of evaporites (Villas et al. 2005) or simple dissolution of evaporite-bearing units.

This study suggests the importance of externally-derived deep-seated formational/metamorphic fluids, possibly with a magmatic component, and meteoric–hydrothermal fluids

for the genesis of IOCG systems in the CMP. This could indicate that the hydrothermal alteration types and the ore signature are strongly controlled by the nature of the host and wallrocks and by the intensity of fluid–rock interactions at different fluid/rock ratios.

Conclusions

The Sossego deposit contains orebodies characterized by distinct types and intensities of alteration and mineralization. A consistent paragenetic sequence of alteration and mineralization is recognized throughout the deposit. This, coupled with similar fluid evolution, sulfur sources, and ore geochemical signatures (iron oxide–Cu–Au–REE–Ni–Co–Pd), suggests a common evolutionary history for different orebodies.

Hydrothermal alteration zones are similar to those recognized as forming at different depths in IOCG deposits worldwide. The Pista–Sequeirinho–Baiano orebodies have undergone regional sodic (albite–hematite) and sodic–calcic alteration controlled by fluid flow in large-scale regional shear zones. These alteration types are similar to those typical of deeper portions of IOCG systems. Massive magnetite–(apatite) bodies were formed by high temperature (>550°C) ^{18}O-enriched (6.9±0.9‰) deep-seated, formational/metamorphic fluids, possibly with magmatic contribution, strongly modified by exchange with magmatic rocks and metavolcano–sedimentary units. Metal and, possibly sulfur, were leached from the host rocks in extensive hydrothermal systems probably driven by heat from intrusions.

Outwards from the high-temperature magnetite-rich bodies, sodic–calcic (6.0±0.8‰, at 500±25°C), and regional sodic alteration (3.6±0.6‰, at 450±50°C) reflect decreasing $\delta^{18}O_{H_2O}$ values, which suggests mixing with ^{18}O-depleted externally derived fluids.

The Sossego–Curral orebodies show the most profound potassic alteration (biotite and potassium feldspar) and chloritic assemblages, similar to those found in high structural levels of IOCG systems. The copper–gold mineralization was late in the alteration history and broadly synchronous in the different orebodies. It was marked by a sharp temperature decrease to below 250°C and influx of D-enriched (δD=−35) and ^{18}O-depleted meteoric–hydrothermal fluids. The ore stage accompanied a transition from ductile–brittle to brittle deformation, which may be associated with decompression due to episodic fluid overpressure. These episodic events might have permitted influx of channeled meteoric water in the system that resulted in dilution and cooling of high-temperature highly saline and metalliferous fluid, causing deposition of metals transported as metal chloride complexes.

Acknowledgments We are grateful to Companhia Vale to Rio Doce for allowing access to the mine and providing logistical support. Special thanks are also due to Márcio Godoy, José J. Fanton, Benevides Aires, Roberta Morais, and José Antonio Garbellotto de Matteo, who provided much of the geological groundwork for this study. We are very grateful to John Humphrey from the Colorado School of Mines (Golden, USA) and Pam Gemery from the U.S. Geological Survey (Denver, USA), who provided the stable isotope analyses. We would especially like to thank Garry Davidson, Patrick Williams, Steffen Hagemann, Erin Marsh, and Byron R. Berger, whose critical comments and suggestions significantly improved the paper. Dailto Silva and Rosane Palissari from the IG–UNICAMP and John Skok from the Colorado School of Mines assisted with the scanning electron microscopy studies. This research has been supported by the Fundação de Amparo à Pesquisa do Estado de São Paulo–FAPESP (Procs. No. 03/01159-1, 04/08126-4, 03-11163-6, 03/09584-3, 03/07453-9), FAPESP/PRONEX 03/09916-6 and FAEP/UNICAMP grants. R.P. Xavier and C.R. Souza Filho acknowledge CNPq for research grants 300579/92-6 and 301.227/94, respectively. M. Hitzman acknowledges support for a portion of this work from the U.S. National Science Foundation under grant EAR-0207217.

References

Albuquerque MAC, Andrade PJMB, Maurity C, Kwitko R (2001) Geologia e características das mineralizações cupríferas do Depósito Alvo 118, Província Mineral de Carajás, Pará, Brasil. Simpósio de Geologia da Amazônia, 7, Belém, SBG, p 5–8 [CD–ROM]

Almada MCO (1998) O Corpo Acampamento Sul do depósito Bahia, Carajás: características geológicas e fluidos hidrotermais. MSc Thesis, Universidade Federal do Pará

Araújo OJB, Maia RGN, Jorge-João XS, Costa JBS (1988) A megaestruturação da folha Serra dos Carajás. Congresso Latino Americano de Geologia 7 Proceedings pp 324–333

Baker T, Perkins C, Blake KL, Williams PJ (2001) Isotopic constraints on the genesis of the Eloise Cu–Au deposit, Cloncurry district, NW Queensland, Australia. Econ Geol 96:723–742

Barros CEM, Sardinha AS, Barbosa JPO, Krimski R, Macambira MJB (2001) Pb–Pb and U–Pb zircon ages of Archean syntectonic granites of the Carajás metallogenic province, northern Brazil. South American Symposium on Isotopic Geology, 3, Proceedings, pp 94–97

Barton MD, Johnson DA (1996) Evaporitic source model for igneous-related Fe oxide–(REE–Cu–Au–U) mineralization. Geology 24:259–262

Beardsmore TJ (1992) Petrogenesis of Mount Dore-style breccia-hosted copper ± gold mineralization in the Kuridala-Selwyn Region of Northwestern Queensland. Unpublished Ph.D. thesis, James Cook University, Townsville, Australia, p 292

Beisiegel VR, Bernardelli AL, Drumond NF, Ruff AW, Tremaine JW (1973) Geologia e recursos minerais da Serra dos Carajás. Rev Bras Geocienc 3:215–242

Berman RG (1991) Thermobarometry using multiequilibrium calculations: a new technique with petrologic applications. Can Mineral 29:833–855

Bernadelli A, Melfi AJ, Oliveira SMB, Trescases JJ (1983) The Carajás nickel deposits. In: Melfi AJ, Carvalho A (eds) IGCP–IUGS–UNESCO Project 129, International Seminary on Laterisation Processs, São Paulo, pp 108–118

Cabral AR, Lehmann B, Kwitko R, Cravo CHC (2002) The Serra Pelada Au–Pd–Pt deposit, Carajas Mineral Province, northern Brazil; reconnaissance mineralogy and chemistry of very high grade palladian gold mineralization. Econ Geol 97:1127–1138

Carvalho ER, Xavier RP, Monteiro LVS, Souza Filho CR, Villas RN, Godoy MLS, Fanton JJ, Nunes AR, Morais R (2004) Geologia do depósito de óxido de Fe–Cu–Au de Sossego, Província Mineral de Carajás (PA). Congresso Brasileiro de Geologia, 42, Proceedings, Araxá, SBG [CD-ROM]

Carvalho ER, Xavier RP, Monteiro LVS, Souza Filho CR (2005) Geology and hydrothermal alteration of the Sossego iron oxide–copper–gold deposit, Carajás Mineral Province, Brazil. In: Simpósio Brasileiro de Metalogenia, 1 [CD-ROM]

Cathelineau M, Nieva D (1985) A chlorite solid solution geothermometer: the Los Azufres (Mexico) geothermal system. Contrib Mineral Petrol 91:235–244

Chacko T, Riciputi LR, Cole DR, Horita J (1999) A new technique for determining equilibrium hydrogen isotope fractionation factors using the ion microprobe: application to the epidote-water system. Geochim Cosmochim Acta 63:1–10

Clayton RN, Mayeda TK (1963) The use of bromide pentafluoride in the extraction of oxygen from oxides and silicates for isotopic analysis. Geochim Cosmochim Acta 27:43–52

Coelho CES, Rodrigues OB (1986) Jazida de manganês do azul, Serra dos Carajás, Pará. In: Schobbenhaus C, Coelho, CES (coords) Principais depósitos minerais do Brasil, Brasília, DNPM/CVRD, v 2, pp 145–152

Cordeiro AAC, Silva AV (1986) Depósito de wolframita da região de Pedra Preta, Pará In: Schobbenhaus C, Coelho, CES (coords) Principais depósitos minerais do Brasil, Brasília, DNPM/CVRD, v 2, pp 409–415

Costa ML (1997) Laterization as a major process of ore formation in the Amazon region. Explor Min Geol 6:79–104

Dall'Ágnol R, Lafon JM, Macambira MJB (1994) Proterozoic anaorogenic magmatism in the Central Amazonian Province, Amazonian Craton: geochronological, petrological and geochemical aspects. Mineral Petrol 50:113–118

Dall'Ágnol R, Souza ZS, Althoff FJ, Barros CEM, Leite AAS, Jorge-João XS (1997) General aspects of the granitogenesis of the Carajás metallogenetic province. Proceedings of the International Symposium on Granites and Associated Mineralizations, Salvador, Excursion Guide, pp 135–161

Dardenne MA, Schobbenhaus CS (2001) Metalogênese do Brasil. Editora Universidade de Brasília/CNPq, Brasília

Dalstra H, Guedes S (2004) Giant hydrothermal hematite deposits with Mg-Fe metasomatism: a comparison of the Carajás, Hamersley, and other iron ores. Econ Geol 99:1793–1800

Davidson GJ, Dixon GH (1992) Two sulphur isotope provinces deduced from ores in the Mount Isa Eastern Succession, Australia. Miner Depos 27:30-41

Dilles JH, Solomon GC, Taylor HP Jr, Einaudi MT (1992) Oxygen and hydrogen isotope characteristics of hydrothermal alteration at the Ann-Mason porphyry copper deposit, Yerington, Nevada. Econ Geol 87:44–63

Docegeo (1988) Revisão litoestratigráfica da Província Mineral de Carajás − litoestratigrafia e principais depósitos minerais. Congresso Brasileiro de Geologia, 35, Belém, SBG, Anexo aos anais, pp 11–54

Dreher AM (2004) O depósito primário de Cu−Au de igarapé Bahia, Carajás: Rochas fragmentárias, fluidos mineralizantes e modelo metalogenético. Ph.D. thesis, Universidade Estadual de Campinas, 221p

Dreher AM, Xavier RP (2005) The Igarapé Bahia deposit, Carajás: A Fe oxide (Cu–Au) hydrothermal system evolved in a submarine Archean setting. In: Simpósio Brasileiro de Metalogenia, 1 [CD-ROM]

Eldridge CS, Compston W, Williams IS, Harris JW, Bristow JW (1991) Isotope evidence for the involvement of recycled sediments in diamond formation. Nature 353:649–653

Eldridge CS, Danti K (1994) Low sulfur isotope rates; high gold values; a closer look at the Olympic Dam Deposit via SHRIMPAbstract with Programs, Geological Society of America 26:498–499

Faraco MTL, Carvalho JMA, Klein EL (1996) Carta metalogenética da Província Carajás -SE do estado do Pará, Folha Araguaia (SB–22) Nota explicativa Belém CPRM

Field CW, Zhang L, Dilles JH, Rye RO, Reed MH (2005) Sulfur and oxygen isotopic record in sulfate and sulfide minerals of early, deep, pre-Main Stage porphyry Cu–Mo and late Main Stage base–metal mineral deposits, Butte district, Montana. Chemical Geology 215:61–93

Fox KA, Hitzman MW (2001) Superimposed magnetite and iron oxide-cu-au mineralization at Productora, Chilean Iron Belt, GSA Annual Meeting

Galarza TMA (2003) Geocronologia e geoquímica iIsotópica dos depósitos de Cu-Au Igarapé Bahia e Gameleira, Província Mineral de Carajás (PA), Brasil. Revista Brasilera de Geociências (RBG Online)

Galarza TMA, Macambira MJB, Moura CAV (2003) Geocronologia Pb–Pb e Sm–Nd das rochas máficas do depósito Igarapé Bahia, Província Mineral de Carajás (PA) Simpósio de Geologia da Amazônia, 7, SBG [CD-ROM]

Garrett SJM (1992) The Geology and geochemistry of the Mt. Elliott Cu-Au Deposit, Northwest Queensland. M.Sc. thesis, University of Tasmania, Hobart p 122

Graham CM, Sheppard SMF, Heaton THE (1980) Experimental hydrogen isotope studies: I Systematics of hydrogen isotope fractionation in the systems epidote–H_2O, zoisite–H_2O and AlO(OH)–H_2O. Geochim Cosmochim Acta 44:353–364

Graham CM, Harmon RS, Sheppard SMF (1984) Experimental hydrogen isotope studies: hydrogen isotope exchange between amphibole and water. Am Mineral 69:128–138

Graham CM, Viglino JA, Harmon RS (1987) Experimental study of hydrogen–isotope exchange between aluminous chlorite and water and of hydrogen diffusion in chlorite. Am Mineral 72:566–579

Haller A, Zúñiga AJ, Corfu F, Fontboté L (2002) The iron oxide-Cu-Au deposit of Raul-Condestable, Mala, Lima, Peru. Sociedad Geologica del Peru (ed), XI Congreso Peruano de Geología, Lima, Resúmenes, p 80

Haynes DW (2000) Iron oxide copper–(gold) deposits: their position in the ore deposit spectrum and modes of origin. In: Porter TM (ed) Hydrothermal iron oxide cooper–gold and related deposits: a global perspective Austral Miner Fund, Adelaide, pp 71–90

Hirata WK, Rigon JC, Kadekaru K, Cordeiro AAC, Meireles EA (1982) Geologia Regional da Província Mineral de Carajás. Simp Geol Amaz, 1, Belém, 1982 Anais Belém, SBG/NO, v 1, pp 100–110

Hitzman MW (2000) Iron oxide–Cu–Au deposits: what, where, when, and why. In: Porter TM (ed) Hydrothermal iron oxide cooper–gold and related deposits: a global perspective Austral Miner Fund, Adelaide, pp 9–25

Hitzman MW, Oreskes N, Einaudi MT (1992) Geological characteristics and tectonic setting of Proterozoic iron oxide (Cu-U-Au-REE) deposits. Precambrian Res 58:241–287

Holdsworth R, Pinheiro R (2000) The anatomy of shallow-crustal transpressional structures: insights from the Archean Carajás fault zone, Amazon, Brazil. J Struct Geol 22:1105–1123

Holland T, Blundy J (1994) Non-ideal interactions in calcic amphiboles and their bearing on amphibole-plagioclase thermometry. Contrib Mineral Petrol 116:443–447

Huhn SRB, Santos ABS, Amaral AF, Ledsham EJ, Gouveia JL, Martins LPB, Montalvão RMG, Costa VC (1988) O terreno granito-greenstone da região de Rio Maria – Sul do Pará In: SBG, Cong Bras Geol, 35, Anais, v 3, pp 1438–1452

Huhn SRB, Souza CIJ, Albuquerque MC, Leal ED, Brustolin V (1999) Descoberta do depósito Cu(Au) Cristalino: Geologia e

mineralização associada região da Serra do Rabo - Carajás – PA. SBG/NO, Simpósio de Geologia da Amazônia, 6, pp 140–143

Huhn SRB, Soares ADV, Souza CIJ, Albuquerque MAC, Leal ED, Vieira EAP, Masotti FS, Brustolin V (2000) The Cristalino copper–gold deposit, Serra dos Carajás, Pará. IUGS, Intern Geol Congr, 31 [CD-ROM]

Hunt J, Baker T, Thorkelson D (2005) Regional-scale Proterozoic IOCG-mineralized breccia systems: examples from the Wernecke Mountains, Yukon, Canada. Miner Deposita 40:492–514

Krcmarov RL (1995) Greenmount Cu-Au-Co Deposit, Cloncurry District. Unpublished M.Sc. thesis, University of Tasmania, Hobart, p 183

Kyser TK, Kerrich R (1991) Retrograde exchange of hydrogen isotopes between hydrous minerals and water at low temperatures. Geochemical Society Special Publication 3:409–422

Lancaster-Oliveira JA, Fanton J, Almeida AJ, Leveille RA, Vieira S (2000) Discovery and geology of the Sossego copper–gold deposit, Carajás District, Pará State, Brazil. In: IUGS, Intern Geol Congr, 31 [CD-ROM]

Ledlie I (1988) Geology of the Teresa de Colmo Fe–Cu breccia deposit. Master of Sciences thesis. Tasmania University, Australia

Leonardos OH, Santos MD, Giuliani G, Araújo LR(1991) The Cumuru mesothermal granodiorite-hosted gold mineralization, Amazon Craton, Brazil In: Ladeira EA (ed) Brazil Gold'91, Balkema, pp 557–562

Lindenmayer ZG (1990) Salobo sequence, Carajás, Brasil: Geology, Geochemistry and Metamorphism. Ph.D. thesis, University of Ontario, Canada, p 407

Lindenmayer ZG (2003) Depósito de Cu–Au do Salobo, Serra dos Carajás: Uma revisão. In: Ronchi LH, Althoff FJ (orgs) Caracterização e modelamento de depósitos minerais. Editora Unisinos, São Leopoldo, pp 69–98

Lindenmayer ZG, Sial AN, Pimentel MM (2002) Composição isotópica dos carbonatos do minério venular do depósito de Cu–Au de Gameleira, Serra dos Carajás, Pará. In: SBG, Congresso Brasileiro de Geologia, 41, Anais, pp 520

Macambira MJB, Lafon JM (1995) Geocronologia da Província Mineral de Carajás: síntese dos dados e novos desafios. Boletim Museu Paraense Emílio Goeldi, Série Ciências da Terra 7:263–288

Machado N, Lindenmayer DH, Krough TE, Lindenmayer ZG (1991) U-Pb geochronology of Archean magmatism and basement reactivation in the Carajás area, Amazon Shield, Brazil. Precambrian Res 49:1–26

Mark G, Williams PJ, Boyce AJ (2004) Low-latitude meteoric fluid flow along the Cloncurry Fault, Cloncurry district, NW Queensland, Australia: geodynamic and metallogenic implications. Chem Geol 207:117–132

Marschik R, Fontboté L (2001) The Candelaria–Punta del Cobre iron oxide Cu–Au (–Zn–Pb) deposits, Chile. Econ Geol 96:1799–1826

Marschik R, Leveille RA (2001) Iron oxide Cu–Au deposits in South America: Candelária, Chile, and Sossego, Brazil. Geological Society of America Abstract with Programs 33

Marschik R, Leveille RA, Martin W (2000) La Candelaria and the Punta del Cobre district, Chile: early Cretaceous iron-oxide Cu–Au(–Zn–Ag) mineralization. In: Porter TM (ed) Hydrothermal iron oxide cooper–gold and related deposits: a global perspective Austral Miner Fund, Adelaide, pp. 163–176

Marschik R, Ryan M, Ruiz J, Leveille RA, Almeida AJ (2002) An Archean Re–Os molybdenite age for the Gameleira Cu–Au–Mo mineralization, Carajas Province, Brazil. Geological Society of America Abstract with Programs 34; 6, p 337

Meireles EM, Silva ARB (1988) Deposito de ouro de Serra Pelada, Maraba, Para. In: Schobbenhaus C, Coelho CES (eds) Principals Depósitos Minerals do Brasil, v. 3. Brasilia, DNPM/CVRD, 547–557

Monteiro LVS, Xavier RP, Carvalho ER, Souza Filho CR, Fanton JJ, Nunes AR, Morais R (2004a) O depósito de óxido de ferro–Cu–Au de Sossego, Carajás: evolução do sistema hidrotermal com base na química mineral e geotermobarometria In: Congresso Brasileiro de Geologia, SBG, 42, Resumos [CD-ROM]

Monteiro LVS, Xavier RP, Carvalho ER, Souza Filho CR, Fanton JJ, Nunes AR, Morais R (2004b) Mistura de fluidos associada à mineralização de óxido de ferro-Cu-Au de Sossego, Província Mineral de Carajás: evidências a partir de isótopos de oxigênio e carbono. In: Congresso Brasileiro de Geologia, SBG, 42, Resumos [CD-ROM]

Morais RPS, Alkmim FF (2005) O controle litoestrutural da mineralização de cobre do Depósito Sequeirinho, Canaã dos Carajás, PA. In: Simpósio Brasileiro de Metalogenia, 1, Gramado, Short Papers [CD-ROM]

Moroni M, Girardi VAV, Ferrario A (2001) The Serra Pelada Au–PGE deposit, Serra dos Carajás (Pará State, Brazil); geological and geochemical indications for a composite mineralising process. Miner Depos 36:768–785

Morrison J (2004) Stable and radiogenic isotope systematics in epidote group minerals. Rev Mineral Geochem 56:607–628

Nogueira ACR (1985) Análise faciológica e aspectos estruturais da Formação Águas Claras, região central da Serra dos Carajás. Master thesis, Universidade Federal do Pará

Ohmoto H (1986) Stable isotope geochemistry of ore deposits. In: Valley JW, Taylor Jr HP, O'Neil JR (eds) Reviews in Mineralogy: Stable isotopes in high temperature geological processes. Mineral Soc Am 16:491–560

Ohmoto H, Rye RO (1979) Isotopes of sulfur and carbon. In: Barnes HL (ed) Geochemistry of hydrothermal ore deposits, 2nd edn. Wiley, New York, pp 509–567

Ohmoto H, Goldhaber MB (1997) Sulfur and carbon isotopes. In: Barnes HL (ed) Geochemistry of hydrothermal ore deposits, 3rd edn. Wiley, New York, pp. 517–611

Oliveira CG, Leonardos OH (1990) Gold mineralization in the Diadema shear belt, northern Brazil. Econ Geol 85:1034–1043

Oreskes N, Einaudi MT (1992) Origin of hydrothermal fluids at Olympic Dam: preliminary results from fluid inclusions and stable isotopes. Econ Geol 87:64–90

Perring CS, Pollard PJ, Nunn AJ (2001) Petrogenesis of the Squirrel Hills granite and associated magnetite-rich sill and vein complex: Lightning Creek prospect, Cloncurry district, northwest Queensland. Precambrian Res 105:213–238

Pimentel MM, Machado N (1994) Geocronologia U-Pb dos terrenos granito-greenstone de Rio Maria, Pará. In: SBG, Cong Bras Geol, Anais, vol 2, pp 390–391

Pimentel MM, Lindenmayer ZG, Laux JH, Armstrong R, Araújo JC (2003) Geochronology and Nd geochemistry of the Gameleira Cu–Au deposit, Serra dos Carajás, Brazil: 1.8–1.7 Ga hydrothermal alteration and mineralization. J South Am Earth Sci 15:803–813

Pollard PJ, Blake KL, Guoyi D (1997) Proterozoic Cu-Au-Co and Pb-Zn-Ag mineralization in the Cloncurry district, eastern Mount Isa Inlier, Australia: Constraints on fluid sources from mineralogical, fluid inclusion and stable isotope data. AMIRA P438 Cloncurry Base Metals and Gold Final Report, Section 7, 50 p

Ramírez LE, Palacios C, Townley B, Parada MA, Sial AN, Fernandez-Turiel JL, Gimeno D, Garcia-Valles M, Lehmann B (2006) The Mantos Blancos copper deposit: an upper Jurassic breccia-style hydrothermal system in the Coastal Range of Northern Chile (in press). DOI 10.1007/s00126-006-0055-9

Réquia KCM, Xavier RP (1995) Fases fluidas na evolução metamórfica do depósito de Cu-Au de Salobo, Carajás, Pará. Revista da Escola de Minas 49:117–122

Réquia K, Fontboté L (2001) The Salobo iron oxide copper–gold hydrothermal system, Carajás mineral province, Brazil. Geological Society of America, Abstract with Programs 33(6):2

Réquia K, Stein H, Fontboté L, Chiaradia M (2003) Re–Os and Pb–Pb geochronology of the Archean Salobo iron oxide copper–gold deposit, Carajá Mineral Province, northern Brazil. Miner Depos 38:727–738

Rigon JC, Munaro P, Santos LA, Nascimento JAS, Barreira CF (2000) Alvo 118 copper–gold deposit—geology and mineralization, Serra dos Carajás, Para, Brazil. In: IUGS, International Geological Congress, 31 [CD-ROM]

Ripley EM, Ohmoto H (1977) Mineralogic, sulfur isotope, and fluid inclusion studies of the stratabound copper deposits at the Raul mine, Peru. Econ Geol 72:1017–1041

Rodrigues ES, Lafon JM, Scheller T (1992) Geocronologia Pb-Pb da Província Mineral de Carajás: primeiros resultados. SBG, Cong Bras Geol, 37, Bol Res Exp, vol 2, pp 183–184

Ronchi LH, Lindenmayer ZG, Araújo JC (2000) Gameleira Cu (Mo-Au) deposit: fluids and hydrothermal alteration (Carajás, Brazil). In: IUGS, International Geological Congress, 31 [CD-ROM]

Rotherham JF, Blake KL, Cartwright I, Williams PJ (1998) Stable isotope evidence for the origin of the Mesoproterozoic Starra Au–Cu deposit, Cloncurry district, northwest Queensland. Econ Geol 93:1435–1449

Savin SM, Lee M (1988) Isotopic studies of hydrous phyllosilicates. In: Hydrous phyllosilicates (exclusive of micas). Rev Miner 19:189–233

Silva ARB, Cordeiro AAC (1998) Depósitos de ouro da Serra das Andorinhas, Rio Maria, Pará. In: Schobbenhaus C, Coelho CES (coords) Principais depósitos minerais do Brasil, Brasília, DNPM/CVRD, v 2, pp 145–152

Soares ADV, Macambira MJB, Santos, MGS, Vieira, EAP, Massoti FS, Souza, CIJ, Padilha JL, Magni MCV (2001) Depósito Cu (Au) Cristalino, Serra dos Carajás, PA: Idade da mineralização com base em análises Pb–Pb em sulfetos (dados preliminares). SBG, Simp. Geol. Amaz., 7, Res. Expandidos [CD-ROM]

Souza LJ, Vieira EA (2000) Salobo 3 Alpha deposit: geology and mineralization. In: Porter TM (ed) Hydrothermal iron oxide copper–gold and related deposits: a global perspective. Australian Mineral Foundation, Adelaide, pp 213–224

Souza SRB, Macambira MJB, Sheller T (1996) Novos dados geocronológicos para os granitos deformados do Rio Itacaiúnas (Serra dos Carajás, PA); implicações estratigráficas. Proceedings of the Simpósio de Geologia da Amazônia, Belém, Brazil, pp 380–383

Souza Filho CR, Carvalho ER, Xavier RP, Monteiro LVS (2004) Unraveling Spectral Signatures of Fe–Ox–Cu–Au Deposits in Carajás (Brazil) through Reflectance Spectroscopy and Aster Imagery Analysis. In: SBG, Congresso Brasileiro de Geologia, 42, Araxá, Resumos [CD-ROM]

Strauss H (1993) The sulfur isotopic record of Precambrian sulfates: new data and a critical evaluation of the existing record. Precambrian Res 63:225–246

Suita MTF (1988) Geologia da área Luanga com ênfase na petrologia do complexo básico-ultrabásico Luanga e depósitos de cromita associados, Pará. Dissertação de Mestrado, Brasília, UnB, p 83

Tallarico FHB, Figueiredo BR, Groves DI, Kositcin N, McNaughton NJ, Fletcher IR, Rego JL (2005) Geology and SHRIMP U–Pb geochronology of the Igarapé Bahia deposit, Carajás copper–gold belt, Brazil: an Archean (2.57 Ga) example of iron–oxide Cu–Au–(U–REE) mineralization. Econ Geol 100:7–28

Tallarico FHB, McNaughton NJ, Groves DI, Fletcher IR, Figueiredo BR, Carvalho BJ, Rego LJ, Nunes AR (2004) Geological and SHRIMP II U–Pb constraints on the age and origin of the Breves Cu–Au–(W–Bi–Sn) deposit, Carajás, Brazil. Miner Depos 39:68–86

Tallarico FHB, Coimbra CR, Cravo Costa CH (2000) The Serra Leste sediment-hosted Au–(Pd–Pt) mineralization, Carajás Province. Revista Brasileira de Geociências 30:226–229

Tavaza E, Oliveira CG (2000) The Igarapé Bahia Au-Cu-(REE-U) deposit, Carajás Mineral Province, Northern Brazil. In: TM Porter (ed) Hydrothermal iron oxide copper–gold & related deposits: a global perspective. Australia Mineral Foundation, Adelaide, pp 203–212

Taylor HP (1968) The oxygen isotope geochemistry of igneous rocks. Contrib Mineral Petrol 19:1–71

Taylor HP Jr (1997) Oxygen and hydrogen isotope relationships in hydrothermal mineral deposits. In: Barnes HL (ed) Geochemistry of hydrothermal ore deposits, Wiley, New York, pp 229–302

Twyerould SC (1997) The geology and genesis of the Ernest Henry Fe–Cu–Au deposit, NW Queensland, Australia. Ph.D. thesis, University of Oregon, p 494

Trendall AF, Basei MAS, De Laeter JR, Nelson DR (1998) SHRIMP U-Pb constraints on the age of the Carajás Formation, Grão Pará Group, Amazon Craton. J South Am Earth Sci 11:265–277

Villas RN, Santos MD (2001) Gold deposits of the Carajás Mineral Province: deposit types and metallogenesis. Miner Depos 36:300–331

Villas RN, Neves M, Sousa F, Lima L, Lamarão C, Xavier R Fanton J, Morais R (2004) Rochas hospedeiras e alteração hidrotermal do depósito Sossego, Província Mineral de Carajás. Congresso Brasileiro de Geologia, 42, Araxá (MG) SBG, Resumos [CD-ROM]

Villas R N, Lima LFO, Neves M P, Sousa FDS, Lamarão CN, Fanton J, Morais R (2005) Relações entre deformação, alteração hidrotermal e mineralização no depósito Cu–Au do Sossego, Província Mineral de Carajás. In: Simpósio Brasileiro de Metalogenia, 1, [CD-ROM]

Williams PJ, Pollard PJ (2003) Australian Proterozoic iron oxide–Cu–Au deposits: An overview with new metallogenic and exploration data from the Cloncurry district, northwest Queensland. Explor Min Geol 10:191–213

Wirth KR, Gibbs AK, Olszewski WJ (1986) U-Pb ages of zircons from the Grão Pará Group and Serra dos Carajás granite, Pará, Brasil. Rev Bras Geocienc 16:195–200

Xavier RP, Wiedenbeck M, Dreher AM, Rhede D, Monteiro LVS, Araújo CEG (2005) Chemical and boron isotopic composition of tourmaline from Archean and Paleoproterozoic Cu–Au deposits in the Carajás Mineral Province. Brazilian Symposium on Metallogeny 1, [CD-ROM]

Zheng YF (1991) Calculation of oxygen isotope fractionation in metal oxides. Geochim Cosmochim Acta 55:2299–2307

Zheng YF (1993a) Calculation of oxygen isotope fractionation in anhydrous silicate minerals. Geochim Cosmochim Acta 57: 1079–1091

Zheng YF (1993b) Calculation of oxygen isotope fractionation in hydroxyl-bearing silicates. Earth Planet Sci Lett 120:247–263

Zheng YF (1994) Oxygen isotope fractionation in metal monoxides. Mineral Mag 58A:1000–1001

Zheng YF (1996) Oxygen isotope fractionations involving apatites: application to paleotemperature determination. Chem Geol 127:177–187